Characterization of the principal tidal current constituents on the Texas-Louisiana shelf

Steven F. DiMarco and Robert O. Reid

Department of Oceanography, Texas A&M University, College Station

Abstract. We analyzed 81 current meter records of varying lengths (3 to 30 months) to describe the principal diurnal (O1, K1, P1, and Q1) and semidiurnal (S2, M2, K2, and N2) tidal current constituents on the Texas-Louisiana continental shelf. The Louisiana-Texas Shelf Physical Oceanography Program (LATEX) had 81 current meters at 31 sites and varying depths from April 1992 to December 1994. The local inertial period range across the shelf (24.4 hours to 26.2 hours) and thermal diurnal cycling during the summer season make it difficult to estimate the diurnal tidal constituents. Dominant tidal modes on the shelf are K1, O1, and M2. Absolute and relative energy contained in each tidal constituent varies with shelf location. The northeast corner of the shelf, near Atchafalaya Bay, has the largest tidal currents with maximum surface current amplitudes (at 3 m depth) of about 9 cm s⁻¹, while typical maximum tidal surface currents near the shelf break are between 1 and 2 cm s⁻¹ for each of the K1, O1, and M2 components. In general, the surface tidal currents decrease in magnitude as water depth increases toward the shelf break, although the semidiurnal components are amplified more at midshelf locations than the diurnal components. Examination of tidal ellipses at different depths suggests that the M2 tide has less vertical structure, while the diurnal tides exhibit more shear, particularly at the more shallow locations. Sea surface height constituents estimated at five locations along the Texas-Louisiana coast are in agreement with historical values.

1. Introduction

The Louisiana-Texas Shelf Physical Oceanography Program (LATEX) had 81 current meters at 31 locations and varying depths along the Texas-Louisiana shelf from April 1992 to December 1994. We analyzed the current meter time series to characterize eight principal tidal current constituents (four diurnal and four semidiurnal) using the iterated least squares method of cyclic descent [Bloomfield, 1976]. Figure 1 shows the configuration of the LATEX current meter array along the Texas-Louisiana shelf. The LATEX array consisted of five cross-shelf transects and two alongshore transects that followed the 50- and 200-m isobaths. The northern edge of the Texas-Louisiana continental shelf is the Texas and Louisiana coast. Gradually sloping seaward, the shelf is bounded by the 200-m isobath at approximately 28°N and 96.3°W, where begins the steep Texas-Louisiana Slope that sharply drops off to more than 1000 m.

The latitude of the shelf moorings defines a range of inertial periods of 24.4 hours at the north and 26.2 hours at the south. This inertial range includes the principal lunar (O1) tide (period = 25.82 hours) and lies very close to the lunar-solar diurnal (K1) and principal solar diurnal (P1) tides, of tidal periods 23.93 and 24.07 hours, respectively. Chen et al. [1996] have shown that near-inertial oscillations represent the largest contribution to the variance for energies between 3 and 40 hours and are generally of the order of the tidal variance. However, Chen et al. [1996] used a very limited portion of the LATEX data set in their investigation of the near-inertial oscillations. Most of the current meter records

Copyright 1998 by the American Geophysical Union.

Paper number 97JC03289. 0148-0227/98/97JC-03289\$09.00

analyzed in that study were of less than 6 months duration and included data recorded during the summer months.

In addition to inertial oscillations, thermal stratification of the surface layer during the summer season (June through August) enhances the excitation of strong oscillations with amplitudes of the order of 20-30 cm s⁻¹ and 24-hour period at some locations on the Texas-Louisiana shelf [*Price et al.*, 1986; also S. F. DiMarco et al., unpublished manuscript, 1997]. At 3 m depth, the amplitudes of these diurnal oscillations can be 10 times the amplitudes associated with the diurnal tidal components. Because much of the data analyzed by *Chen et al.* [1996] included summer data, their analysis was contaminated by the effects of diurnal cycling. We use a least squares harmonic analysis of time series that includes gaps to minimize the nontidal contributions near diurnal periods. Table 1 shows the eight tidal periods analyzed.

Historically, the tides of the Gulf of Mexico are considered to be comparatively small relative to oceanic tides. Marmer [1954] characterized these to range from principally diurnal (one high and one low tide per day) to mixed diurnal. The mixed tide has two high and low tides per day [Rezak et al., 1985], but with a large difference between the two highs and two lows. A model study by Reid and Whitaker [1981] has shown the principal semidiurnal M2 tide to be a Kelvin wave which propagates cyclonically in the Gulf basin around an amphidromic point north of the Yucatan peninsula. The Gulf response to the M2 tide is much greater to the direct tidal potential forcing than to the open boundary forcing provided by the flow through the Florida Straits and the Yucatan Channel [Reid, 1990]. The Gulf diurnal tide, however, is cooscillating with the Atlantic tide and is driven by the in-phase flow into the Gulf basin through the Florida Straits and the Yucatan Channel. The natural (Helmholtz) mode of oscillation

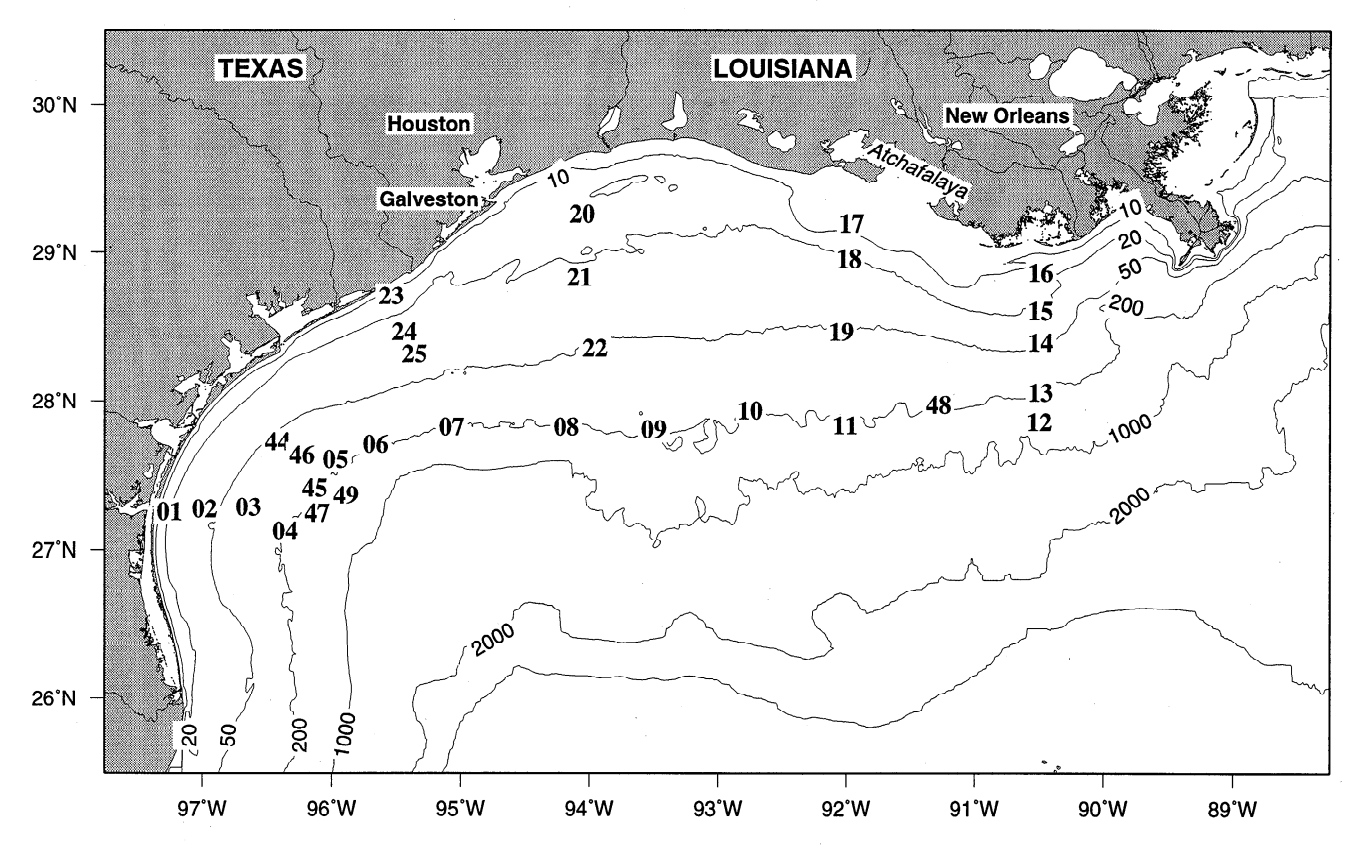


Figure 1. Texas-Louisiana shelf showing LATEX current meter locations and 10-, 20-, 50-, 200-, and 1000-m isobaths.

has been estimated by *Mofjeld and Wimbush* [1977] to be ~1.5 days based on observation.

Current ellipses for each tidal constituent were constructed from the north-south and east-west current components. The ellipses generally are aligned across the bathymetry, except for stations close to the coast and the eastern most stations, and increase in amplitude with proximity to the shore. The tidal ellipses for the semidiurnal tidal current constituents are more oblate than those estimated for the diurnal constituents. The near-surface M2, K1, and O1 tides are anticyclonically rotating. Strong vertical shear is apparent in the maximum tidal amplitudes of the three major diurnal tidal current constituents, while the semidiurnal tidal current constituents showed little evidence of shear, particularly at larger depths. The main variability of the M2 tide is with horizontal location on the shelf.

Not addressed in this paper is a quantitative analysis of the baroclinic structure of the tidal currents due to the low

Table 1. Periods of Principal Tidal Constituents

Symbol	Name	Period, solar hours
	Semidiurnal	
M2	principal lunar	12.42060
S2	principal solar	12.00000
N2	larger lunar elliptic	12.65835
K2	luni-solar semidiurnal	11.96724
	Diurnal	
K1	luni-solar diurnal	23.93447
01	principal lunar diurnal	25.81934
P1	principal solar diurnal	24.06589
Q1	larger lunar elliptic	26.86836

horizontal and vertical spatial resolution of the current meter array, or the contribution of internal waves generated near the shelf break by tidal currents on a stratified shelf. *Li et al.* [1997] discuss the mean hydrographic fields and their interannual variability over the Texas-Louisiana shelf.

A description of the data and the methodology used to estimate the principal tidal current constituents on the Texas-Louisiana shelf is given in section 2. Section 3 discusses the estimated semidiurnal tidal current constituents, followed by the diurnal tidal current constituents, and lastly, a description is given of the principal sea surface height tidal constituents at five mooring locations. A closing summary is given in section 4.

2. Methodology

The method of cyclic descent (MCD) was used to determine tidal amplitudes and phase based on an iterated least squares method [Bloomfield, 1976]. This method optimizes the phase and amplitude of a given frequency of the time series at each location including time series which contain gaps. By using a least squares harmonic analysis, the stationary (deterministic) tides can also be adequately separated from the randomly phased inertial (wind-driven) events if sufficiently long time series are available. To reduce the total time series variance and obtain the most accurate estimates for the tidal constituents, the data were 3- to 40-hour band-passed filtered and sampled at a period of 1 hour. Data gaps in the raw record of less than 6 hours (gaps mainly due to instrument replacement) were filled using linear interpolation, while gaps of less than 2 weeks were filled using a maximum entropy

(spectral-preserving) method. Data gaps longer than 2 weeks were not filled. Continuous time series segments of 512 hours and greater after filling at each location were used to estimate the energy spectrum.

The large amplitudes of the diurnal oscillations continue to contaminate the estimates for the diurnal constituents despite a least squares analysis. Therefore, to minimize the contamination of the summer diurnal oscillations enhanced by the solar heating of the surface layer, all time series during June, July, and August were excluded from the analysis. Two mooring locations, 45 and 47, were completely eliminated from this analysis because their time series occurred almost entirely during the summer months of 1992.

Eight tidal frequencies were estimated: four diurnal (O1, K1, P1, and Q1) and four semidiurnal (M2, S2, K2, and N2). To estimate the maximum tidal kinetic energy, the maximum tidal amplitudes of the tidal ellipses were constructed from the north-south and east-west amplitudes estimated from the method of cyclic descent. The root-mean-square of the maximum variance of the eight tidal constituents provides a rough estimate of the mean tidal current at each location.

Another computational method to determine the tidal kinetic energy is to estimate the energy spectrum of the raw 3-hour low-passed hourly time series using a fast Fourier transform (FFT) and then remove the tides from the raw time series by subtracting a sine curve with the appropriate amplitude and phase of each tidal constituent. An FFT is then done on the resulting detided time series. The difference in energy between the integrated raw FFT and detided FFT results in an estimate for the total energy due to the eight main tidal current constituents. This method was used to determine the ratio of tidal energy to total energy in the 3- to 40-hour energy band.

Tidal ellipses were constructed from the phase and amplitudes of the north-south and east-west components of each tidal current constituent. The major (M) and minor (m) axes of the tidal current ellipse for a given constituent are defined as [Godin, 1972]

$$M = \frac{1}{2} \left[\sqrt{(a_u + b_v)^2 + (a_v - b_u)^2} + \sqrt{(a_u - b_v)^2 + (a_v + b_u)^2} \right]$$

$$+ \left[\frac{1}{2} \sqrt{(a_u + b_v)^2 + (a_v - b_u)^2} - \sqrt{(a_u - b_v)^2 + (a_v + b_u)^2} \right],$$
(1a)

respectively. The subscripts u and v designate the east-west and north-south current components, respectively. The angle of the major axis relative to the east-west axis is

$$\alpha = \frac{1}{2} (\alpha_1 + \alpha_2), \tag{2}$$

where α_1 and α_2 are defined by:

$$\alpha_1 = \tan^{-1} \left(\frac{a_v - b_u}{a_u + b_v} \right). \tag{3a}$$

$$\alpha_2 = \tan^{-1} \left(\frac{a_v + b_u}{a_u - b_v} \right). \tag{3b}$$

The *n*th tidal constituent is defined by $A_n \exp \left[i(\omega_n t - \phi_n)\right]$, where A_n , ω_n , and ϕ_n are the amplitude, frequency, and phase, respectively. The a and b terms are related to the amplitude and phase of the tidal current constituents by $a = A \cos \phi$ and $b = -A \sin \phi$ and are directly determined from the MCD analysis

As stated earlier, the current velocity data recorded during the summer months were removed from our analysis to avoid the contamination by thermally induced diurnal oscillations. Figure 2 shows spectral densities of the along-shelf and cross-shelf current velocity components at site 22 (instrument at 3-m depth) estimated during the summer and nonsummer months between April 1992 and November 1994. We see that the energy in the diurnal frequency band of both components is about 1 order of magnitude larger in the summer than in nonsummer. The energy in the semidiurnal band is approximately the same for both summer and nonsummer. Figure 2 is representative of all current meter data recorded during the LATEX program. However, the disparity in summer and nonsummer diurnal energy is greatest for the near-surface instruments and decreases for instruments deeper in the water column.

We note that the tidal current amplitude and Greenwich phase estimates presented in this paper are corrected following Godin [1972] and Foreman [1977] for the astronomical argument and nodal modulation, f. The nodal correction was determined by estimating the mean f for each constituent during the length of the time series and dividing the amplitudes obtained from the MCD analysis by this mean f. The Greenwich phase lag is determined from $G_i = (V_o + u)_i - 0.5 \cdot (\alpha_{I_i} - \alpha_{2_i})$, where the equilibrium phase, $(V_o + u)$, is determined using tables given by Schureman [1976].

We present Table 2 as a comparison between the tidal ellipses estimated using the method of cyclic descent and those estimated using a tidal analysis code by Foreman [1977] and Foreman et al. [1995]. Shown are the semimajor and semiminor axis amplitudes and directional orientation of the semimajor axis relative to north. The amplitudes estimated from both the Foreman code and MCD have not been nodally modified and represent the average tidal ellipse over the study period (excluding summers) so that we can directly compare the output of the least squares analysis. We see that the agreement is very good for the largest principal components (M2, O1, and K1) in both magnitude and orientation. The orientation difference is greatest in the very small K2 amplitude, which is well within the residual noise error of the calculation. The least squares error associated with the MCD and Foreman estimates is approximately 0.38 cm s⁻¹,

3. Results and Discussion

The method of harmonic analysis described above was performed on the time series observed at each current meter station. The main tidal current constituents were found to be M2, S2, O1, K1, and P1. Together they account for an average of 92% of the total tidal variance estimated from the maximum amplitudes of the eight tidal current constituents. Maximum M2, K1, and O1 amplitudes were approximately the same order of magnitude and account for an average of 76% of the total near-surface tidal energy at the LATEX sites. Figure 3 shows contours of the percentage of total tidal energy for the eight analyzed tidal current constituents to total energy variance in the 8- to 40-hour energy band for the LATEX surface instruments (essentially at 10-m depths). The percentages were de-

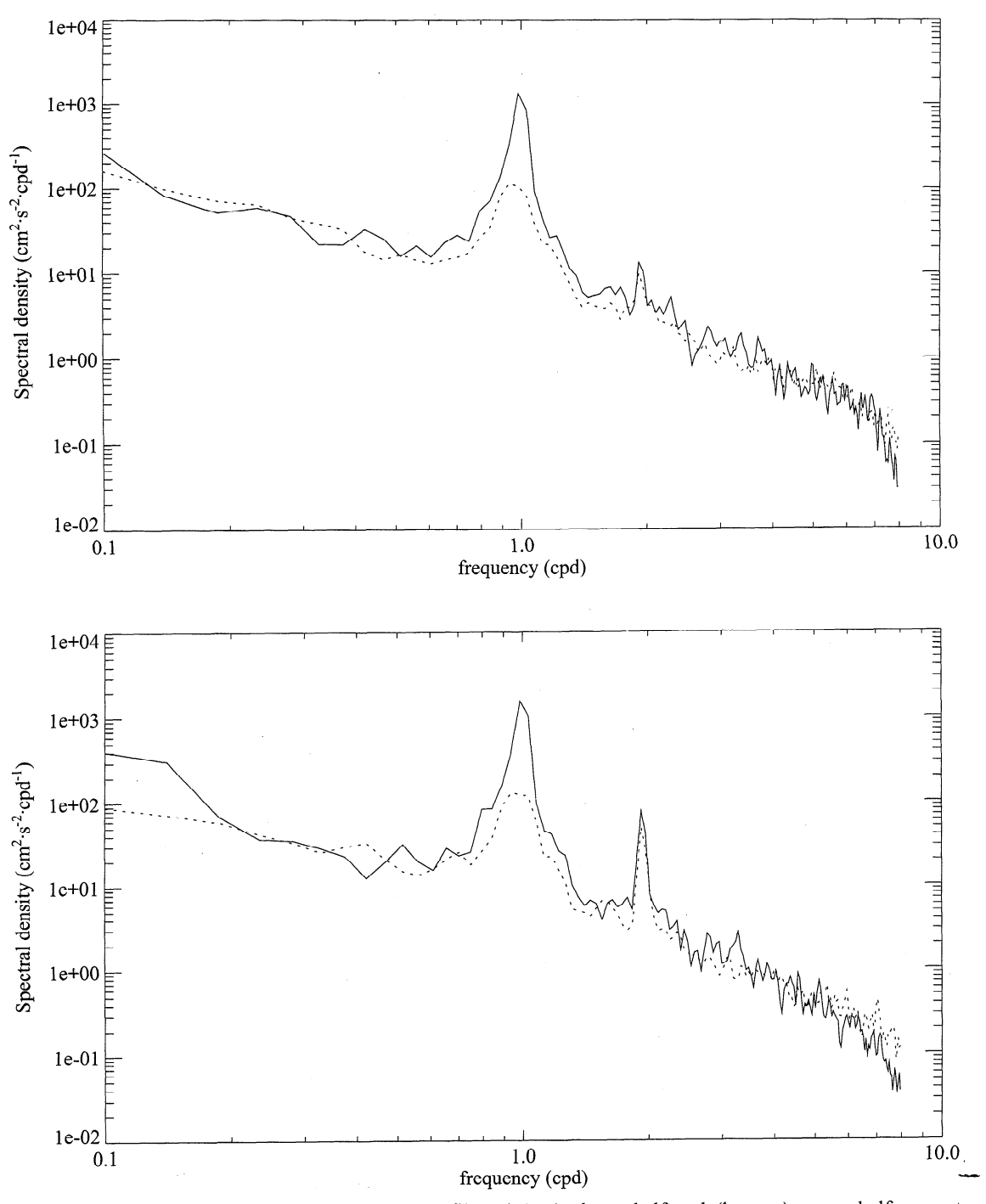


Figure 2. Spectral density of 3-hour low-pass filtered (top) along-shelf and (bottom) cross-shelf current velocity during summer (solid) and nonsummer (dashed) months at site 22 (3-m depth) from April 1992 to November 1994.

termined by comparing the ratio of the raw time series with a residual time series after the tidal constituents were removed. At the shelf edge (along the 200-m isobath), the tidal energy accounts for less than 10% of the total variance. The percentage of tidal energy increases closer to shore and in the wider regions of the shelf. The percentage is greatest in the shallow region southwest of Atchafalaya Bay, where it exceeds 40%. There is also a local maximum in this ratio at the surface meter at site 21 in the central shelf southeast of Galveston, which is

attributed to low amounts of nontidal energy in the 8- to 40-hour energy band.

3.1. Semidiurnal Tidal Currents

This section summarizes the results for the semidiurnal tidal current constituents. Table 3 lists the major and minor axis magnitudes, directional orientation of the major axis relative to north, and phase lag relative to Greenwich. The sign of the

		Foreman	MCD			
Tide	Major Axis, cm s ⁻¹	Minor Axis, cm s ⁻¹	θ, °N	Major Axis, cm s ⁻¹	Minor Axis, cm s ⁻¹	θ, °N
M2	5.66	1.76	3	5.64	1.81	4
S2	1.73	0.45	179	1.75	0.47	182
N2	1.40	0.42	2	1.42	0.43	2
K2	0.15	0.11	103	0.15	0.07	332
K1	3.20	2.82	7	3.75	3.00	13
O1	3.28	2.72	9	3.23	2.70	6
P1	1.31	0.94	9	1.14	0.73	6

100

0.84

Table 2. Comparison of Principal Tidal Current Ellipses Estimated From Foreman Code and MCD (Site 21 Top)

MCD denotes method of cyclic descent.

0.78

0.84

minor axis indicates the sense of rotation of the tidal current vector: positive for cyclonic rotation, negative for anticyclonic rotation.

Q1

The M2 tide dominated the semidiurnal energy band (11 to 14 hours) of the energy spectrum at all stations. Figure 4 shows a plan view of the M2 tidal current ellipses estimated from the upper current meter at each location. The depths of the LATEX surface current meters were generally 10 m, except for sites 17, 19, 20, 22, which were at 3 m. The current ellipses are generally oriented with major axes across the bathymetry lines at the shelf edge and are rotating anticyclonically. The ellipse at site 20 collapses to a straight

line, indicating that there are equal magnitudes of right circularized current and left circularized current [Gonella, 1972]. At the easternmost cross-shelf line, the M2 tidal ellipses are oriented nearly parallel to the bathymetry, primarily due to the narrowing of the shelf and the stations' proximity to the Mississippi Canyon to the east. The tidal ellipses along latitudes 92°W and 95.5°W are also at an angle to the bathymetry and tend to favor an orientation that is slightly more parallel to the coast. Specifically, the tidal ellipse at site 23 is almost parallel to the coast due to its proximity to shore and shallow depth. The tidal ellipses along the cross-shelf lines of 94°W (midshelf line) and the

95

0.78

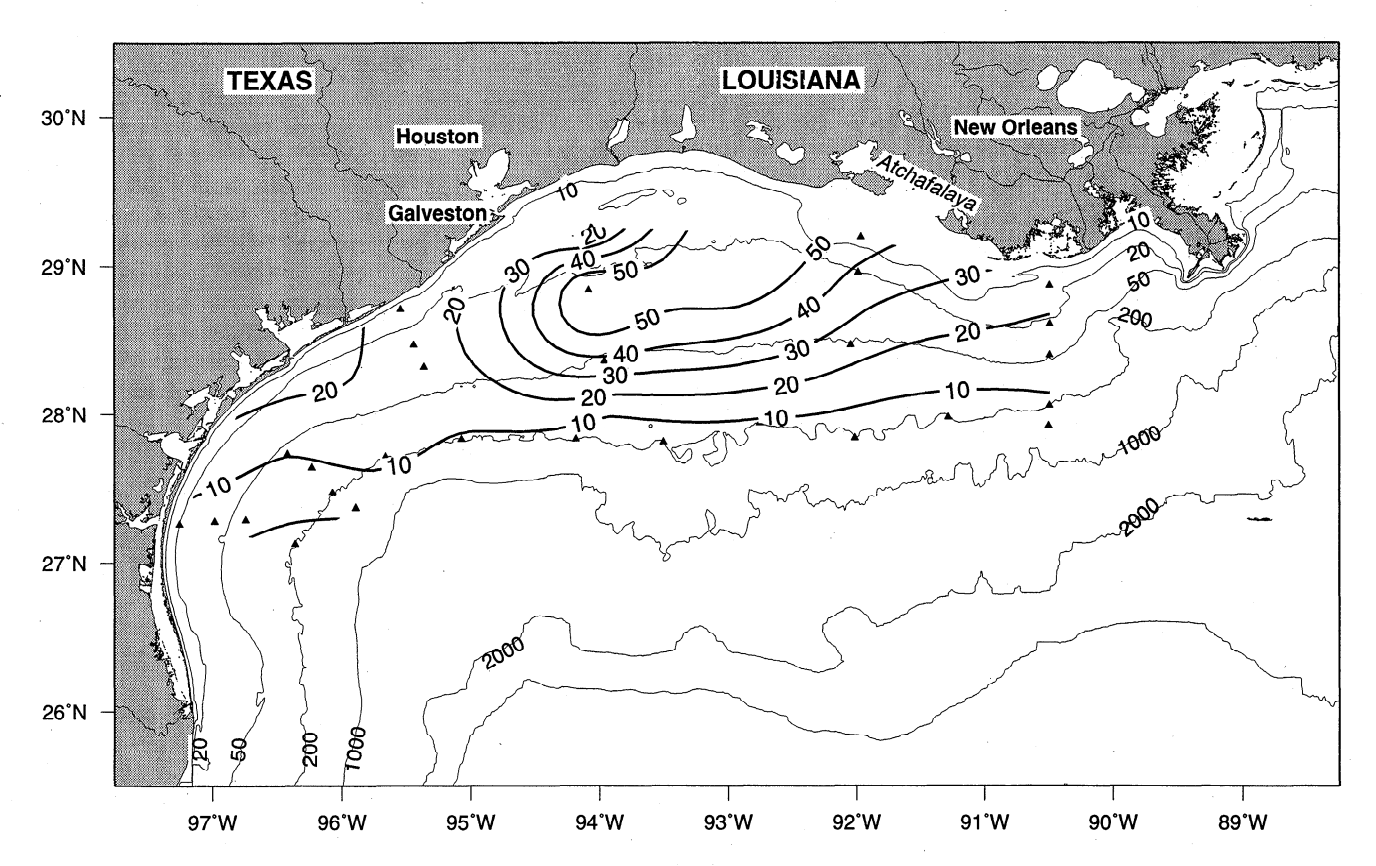


Figure 3. Percentage of energy associated with eight principal tidal current constituents relative to total energy in the 8- to 40-hour energy band for upper instruments. Triangles represent current meter locations. Contour interval is 10.

Table 3. M2 Tidal Current Ellipses at LATEX Current Meter Locations

Site Depth, A G, Hours Major, Minor Number cm s⁻¹ cm s-1 °N m 01 10. 10038. 0.50 -0.23 300. 12. 01 12. 5740. 0.20 -0.0174. 161. 290. 02 10. 15674. 1.00 -0.531. 301 166 02 9084. 0.75 -0.2032. 03 10. 12808. 0.82 -0.54299. 176. 03 33. 6268. 0.97 -0.42310. 178. 03 58. 7620. 0.90 -0.34302. 165. 297. 04 14. 12345. 0.50 -0.1023. 302. 170. Λ4 100 -0.1313258. 0.55 04 190. 11807. 0.59 -0.27 304. 11. 05 9310. 0.36 -0.06 332. 21. 14. 313. 05 100. 12405. 0.42 -0.21165. 0.22 05 190. 10596. -0.15304. 327. 17. 06 15136. 1.14 -0.6914. 06 100. 13447. 0.69 -0.35333. 10. 190. 5949. 0.18 0.02 49. 169. 06 351. 07 14. 10982. 1.20 -0.64 34. 100. 348. 26. 07 7224. 0.69 -0.14 07 -0.78360. 176. 190. 12800. 1.82 08 14. 15045. 1.66 -0.85347. 179. 08 100. 12846. 1.16 -0.46347. 11. 0.17 303. 114. 190. -0.0208 11667. 09 9933. 1.42 -0.51 332. 20. 14. 100. 14413. 341. 7. 09 0.83 -0.1809 13013. 357. 154. 190. 0.70 -0.2110 14. 10245. 2.16 -0.79336. 163. 100. 332. 176. 10 15473. 1.19 -0.2615406. -0.09 25 61 10 190 0.66 13752. -0.24324. 159. 11 14. 1.02 100. 12746. 1.05 -0.13313. 149. 11 150 11 190. 7113. 1.47 -0.07340 9798. 274. 170. 12 14. 0.82 -0.15100. 82. 178. 6230 0.01 12 0.61 275. 12. 12 490. 5401. 0.25 0.00 13 14328. 0.95 -0.2887. 154. 14. 72. 170. 100. 0.51 0.30 13 15725. 62. 13 190. 11357. 0.82 0.32 346. 299. 123. 12287. 1.13 0.15 14 10. 14 26. 11257. 0.96 0.15 272. 133. 14 40. 6895. 1.07 0.21 83. 140. 15 10. 15708. 1.48 0.01 289. 118. 10509. 15 17 303. 1.57 -0.0597. 113. 10. 11879. 1.98 16 -0.10283. 16 14. 7653. 1.54 0.04 291. 80. 17 7406. 140. 3. 9.45 -4.87 357. 17 6. 9382. 6.60 -2.48357. 149. 18 8. 11529. 4.56 -1.57338 150. 19. 18 9003. 3.86 -0.70349. 141. 7396. 329. 19 3. 3.25 -0.89 119. 19 20. 6404 344. 2.11 -0.61160. 19 45. 9573. 2.72 -0.64337. 145. 20 3. 10754. 4.15 0.24 3. 159. 3.25 20 13. 11457. 0.55 7. 155. 21 14. 16245. 5.56 -1.79 4. 22. 10681. 166. 21 4.05 -0.796. 22 3. 10356. 3.67 -1.13148 22 20. 13677. 3.02 -0.99359. 2. 22 7849. 48 3.44 -1.073. 176. 23 10. 12342. 2.29 -0.4351. 28. 23 13. 6043. 1.83 -0.3248. 7. 13028. 24 10. 2.67 -1.0427 32 1.99 24 9939. -0.69 23. 179. 25. 25 11 7705 2 72 11. 25. -1.3625 20. 7851. 2.87 -1.35 9. 24. 12. 25 29. 4952. 2.69 -0.9615. 310. 145. 44 13. 3452. 1.01 -0.65 29. 44 55. 2187. 0.88 -0.27320. 17. 46 14. 4442. -0.46337 1 36 3271. 0.77 -0.24336. 31. 50.

Table 3. (continued)

Site Number	Depth, m	Hours	Major, cm s ⁻¹	Minor, cm s ⁻¹	θ, °N	G,
46	84.	2164.	0.96	-0.50	324.	170.
48	14.	13556.	1.03	0.00	312.	129.
48	100.	13519.	0.63	0.23	311.	153.
48	190.	7204.	0.66	0.50	324.	102.
49	14.	10618.	0.46	-0.23	275.	69.
49	100.	11523.	0.08	-0.01	344.	140.
49	490.	11341.	0.31	-0.10	329.	164.

westernmost cross-shelf line are oriented across the bathymetry. This figure provides qualitative verification of the tidal model of *Reid and Whitaker* [1981], particularly at the inner shelf and eastern region near Mississippi Canyon where the observed orientations and magnitudes agree with the model results for the M2 tidal current ellipses [Rezak et al., 1985].

Figure 4 and similar additional figures of tidal ellipses of other constituents also provide estimates for the least squares error and phase for each estimate. The shaded region depicted around the estimated tidal hodograph corresponds to the least squares error due to the presence of the residual (detided) time series and provides an estimate for the accuracy and confidence for the tidal amplitudes. The least squares error was calculated for each velocity component and assumes a decorrelation timescale of 72 hours for the residual time series.

Phase information is depicted as a solid circle on each tidal ellipse signifying the direction of the current vector at an arbitrary time (chosen to be 0000 UTC, April 7, 1992). Together these solid circles essentially represent a synoptic snapshot of the tidal vectors. It has been shown in the model study by Reid and Whitaker [1981] that the M2 sea surface height propagates cyclonically (counterclockwise) around the Gulf of Mexico basin with an amphidromic point north of the Yucatan peninsula. Quantitative interpretation of the phase is difficult because of the error associated with both the amplitude and orientation of the current ellipse. However, the phase of the M2 tidal currents provides qualitative verification of that model, in that there is a time lag between the M2 tidal vectors of the western stations relative to those in the east. The phase angle should be considered relative to a local bathymetric (along- and cross-shelf) coordinate system.

Along the shelf break, an average of 19.4% of the total tidal variance was attributable to the M2 tide. This average percentage increased closer to shore to 24%, 30%, and 31% for instruments near the 50-m isobath, near the 20-m isobath, and the shallowest mooring location of each cross-shelf mooring line, respectively. On average over the entire shelf, the M2 tidal current was 21.8% of the total tidal variance. The percentage of total tidal variance due to the S2, N2, and K2 tides was generally less than 5 across the shelf.

Figure 5 shows contours of the maximum M2 tidal amplitudes (magnitude of semimajor axis) for the surface current meters on the LATEX shelf. At midshelf the contours run parallel to the bathymetry and have the largest values near the coast, particularly at site 17, southwest of the Atchafalaya Bay, where the M2 tidal current has a maximum value of 9.6 cm s⁻¹. Clarke and Battisti [1981] (henceforth referred to as CB) have shown that barotropic semidiurnal tides can be strongly amplified on wide continental shelves whereas diurnal tides are rarely strongly amplified. As the shelf narrows on either side,

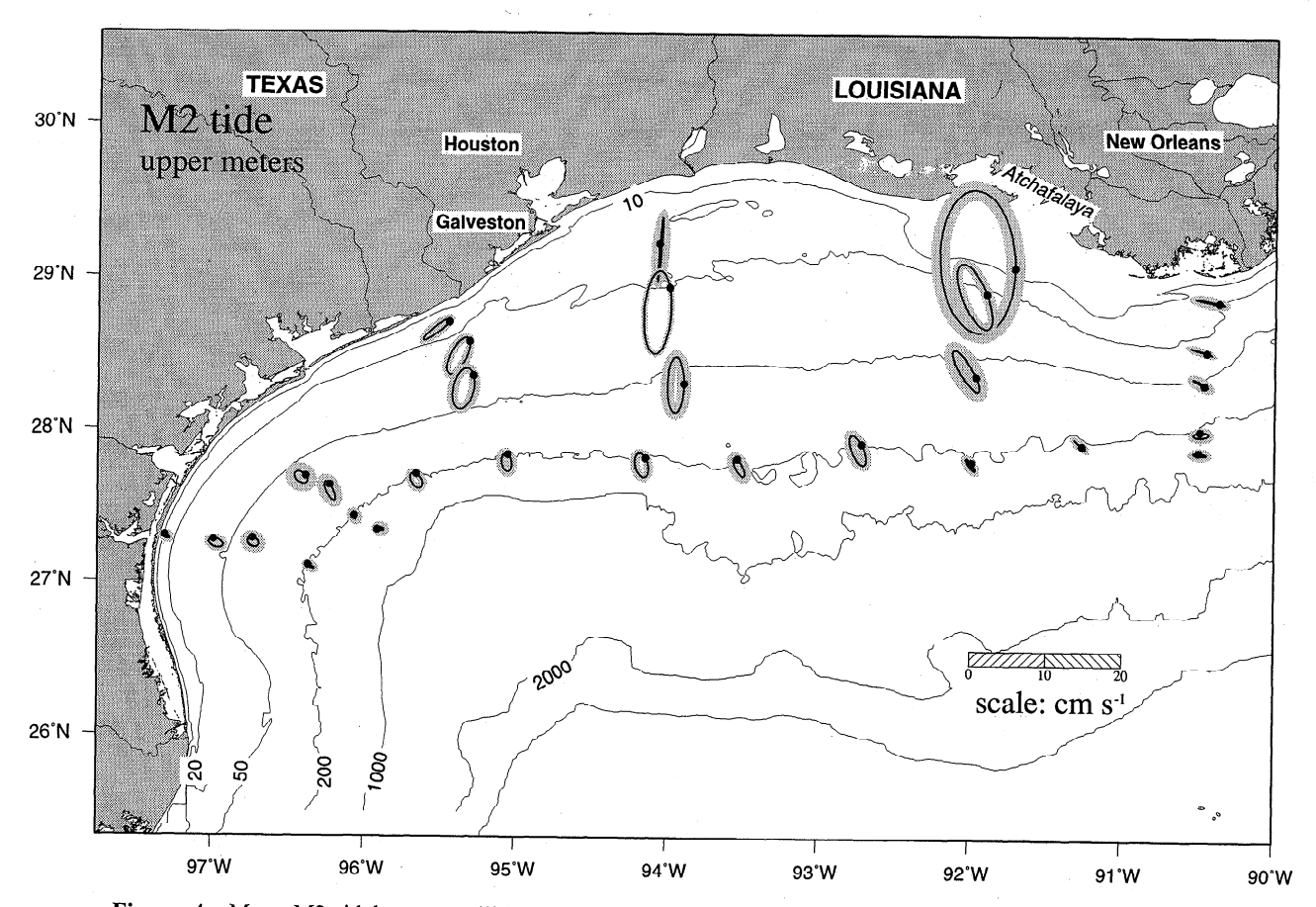


Figure 4. Mean M2 tidal current ellipses during the period April 1992 to December 1994 for upper current meters showing orientation of tidal current vectors at 0000 UTC, April 7, 1992 (solid circle) and least squares error estimate (shaded).

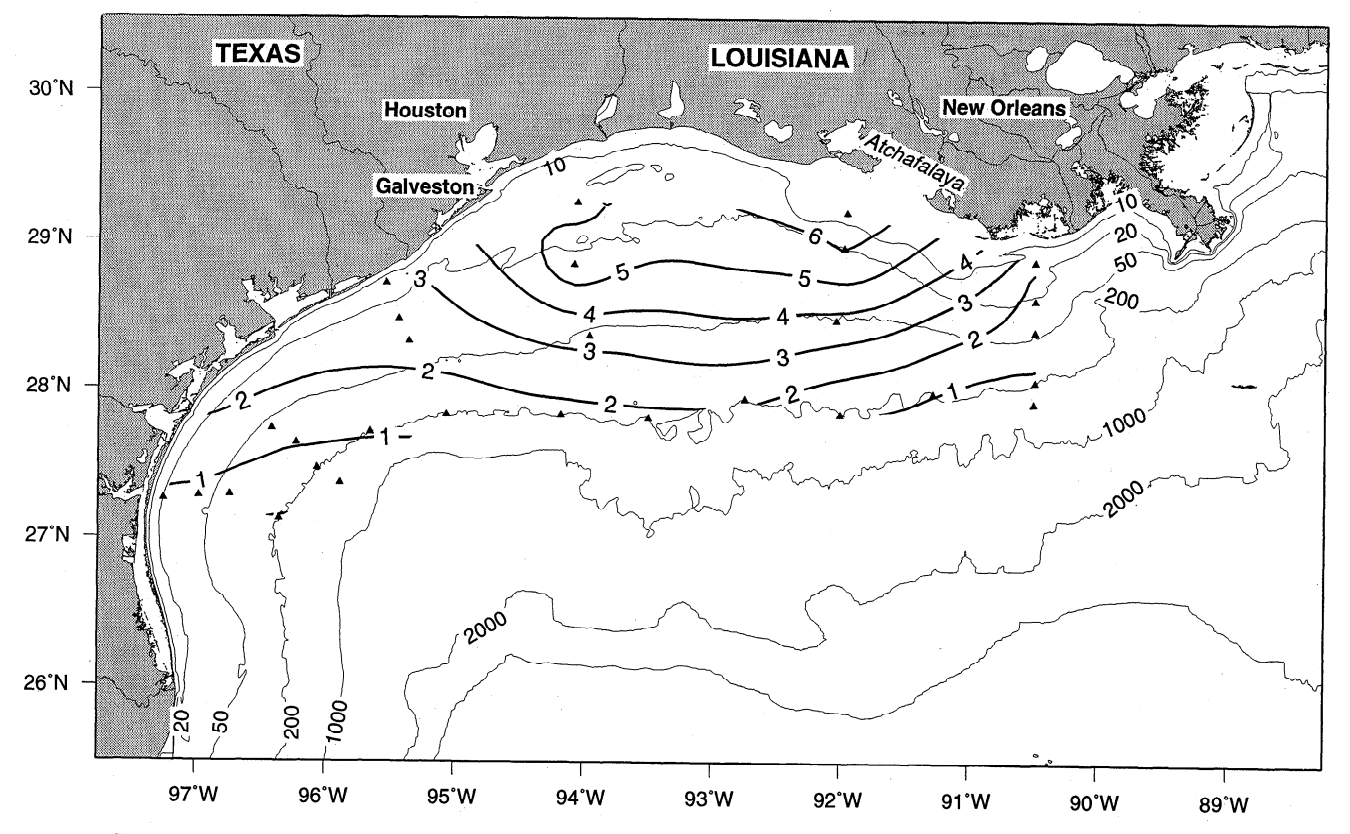


Figure 5. Contour of maximum M2 tidal current amplitudes for upper current meters. Triangles represent current meter locations. Contour interval is 1 cm s⁻¹.

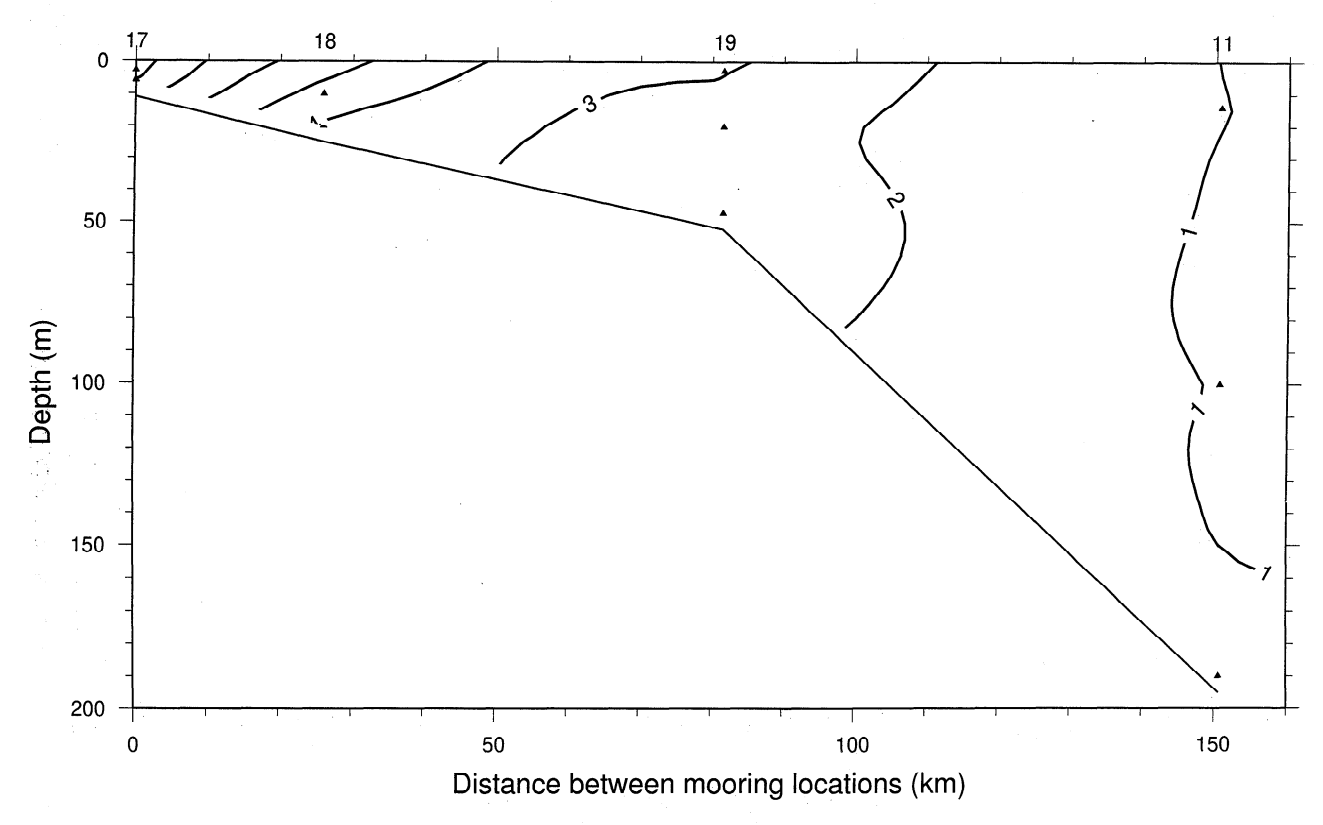


Figure 6. Vertical profile of maximum M2 tidal current amplitudes for current meters along 92°W. Triangles represent locations of current meters in water column. Mooring number is given at the top of the figure. Contour interval is 1 cm s⁻¹.

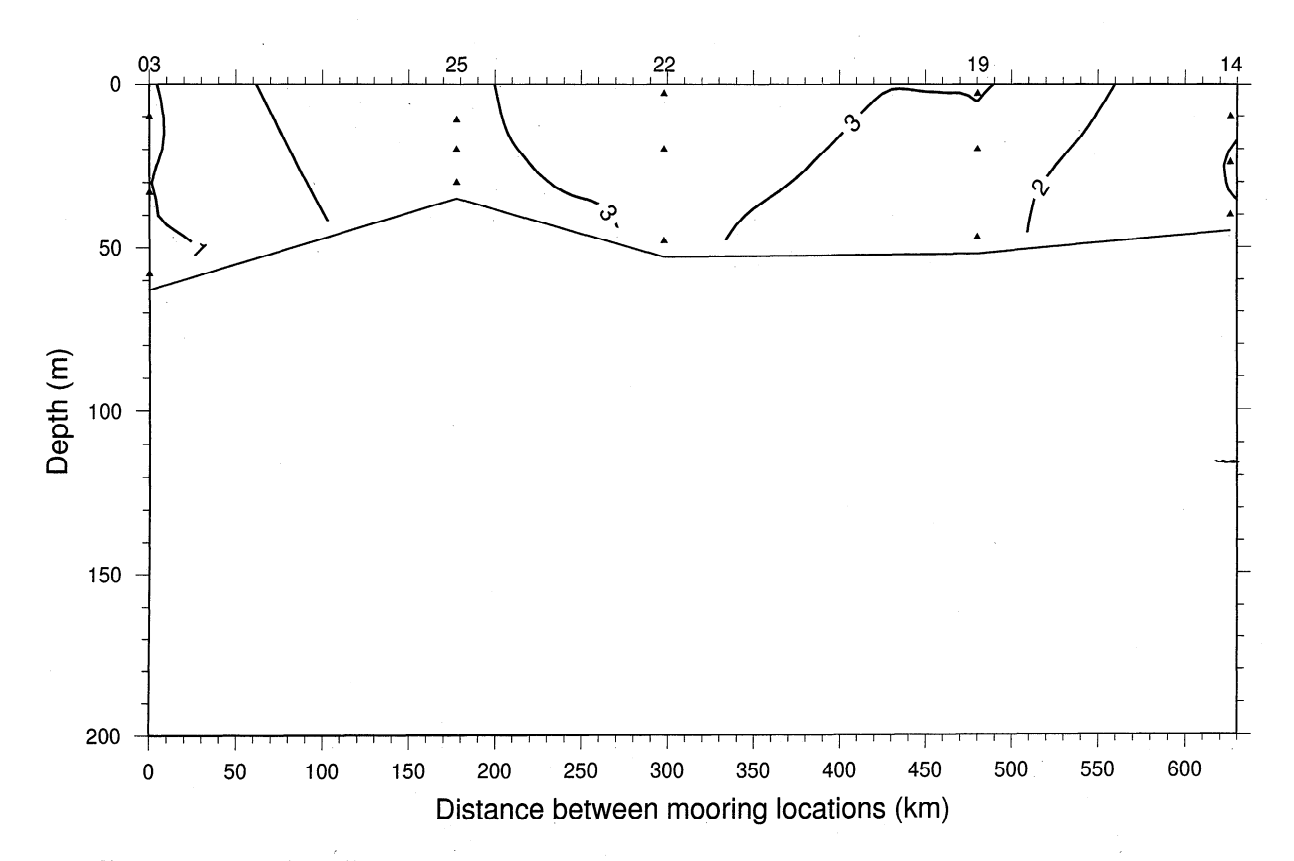


Figure 7. Vertical profile of maximum M2 tidal current amplitudes for current meters along 50-m isobath. Triangles represent locations of current meters in water column. Mooring number is given at the top of the figure. Contour interval is 1 cm s⁻¹.

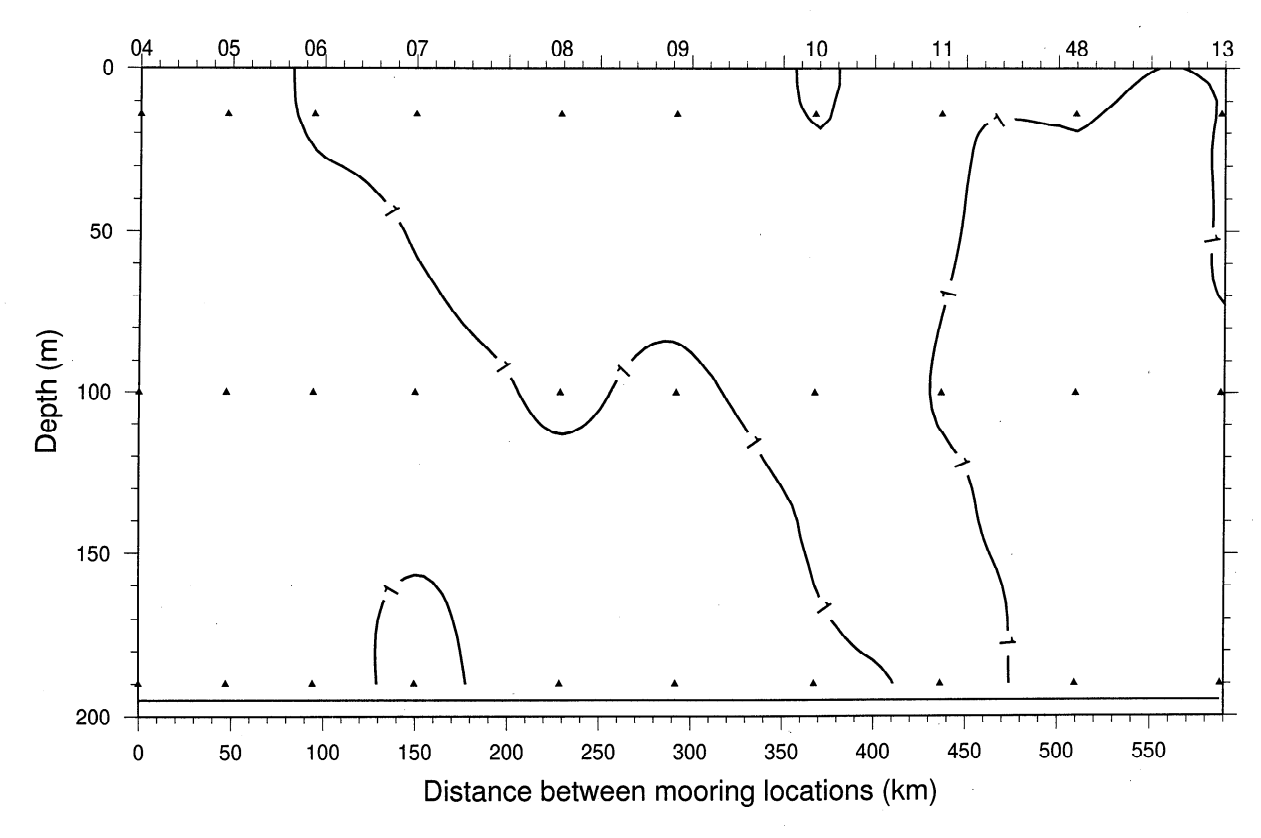


Figure 8. Vertical profile of maximum M2 tidal current amplitudes for current meters along 200-m isobath. Triangles represent locations of current meters in water column. Mooring number is given at the top of the figure. Contour interval is 1 cm s⁻¹.

the contours run at larger angles to the bathymetric lines. The maximum amplitude of the M2 tide at the shelf edge is about 2 cm s⁻¹. As the shelf bends southward in the western region, the contours are perpendicular to the bathymetry and have magnitudes less than 1.5 cm s⁻¹. Similarly, at the eastern shelf the M2 tidal current is less than 1.5 cm s⁻¹ except for site 16 just south of Terrebonne Bay, which was slightly over 2 cm s⁻¹.

Similar behavior was seen for the S2, K2, and N2 tidal currents, with generally larger amplitudes at midshelf and a steady decrease toward the shelf break and the eastern and western boundaries. However, the amplitudes of these tidal currents were generally much smaller than the M2 amplitudes.

Measurements of the M2 tidal current made at the Flower Gardens Bank (15 km southwest of site 09) from March 6 to April 4, 1981, using an electromagnetic current meter at a depth of 97 m, show the north-south M2 tidal current component to be 1.9 cm s⁻¹ [Rezak et al., 1985]. This may be compared with the maximum north-south M2 tidal current of 0.8 cm s⁻¹ estimate in the present study at site 09 at 100-m depth. Note, however, that the 1981 estimate is based on only one month of record, as compared to 20 months in the present analysis.

Figure 6 shows a cross section of the maximum M2 tidal current amplitudes on the cross-shelf line which follows the 92°W meridional line. The M2 tide shows little evidence of vertical shearing beyond the 50-m isobath. The contours become more inclined in the shallower region near site 17 as

bottom friction plays a larger role in the shallow water near the coast. This line is representative of the other cross-shelf lines at 92.5°W and 95.5°W. The general pattern is slightly changed for the line along 94°W where there is a surface maximum at site 21 (Figure 5).

The vertical east-west cross section along 27.25°N (not shown) has very little vertical or horizontal variation, indicating a barotropic M2 tidal current across the shelf in this region. This is generally true of all four principal semidiurnal tidal current constituents in this region.

Figure 7 shows a vertical section along the 50-m isobath of the M2 tidal current. Again we see nearly vertical contours (barotropic) and maximum amplitudes at midshelf (in accordance with CB theory). There is some evidence of shear at the upper current meters of the inner shelf, particularly for the S2 tide. The other semidiurnal tidal constituents behave similarly to the M2 tide along the 50-m isobath. The Reid and Whitaker model results for the M2 tidal current also indicate along-isobath variation similar to that seen in Figure 7 [Rezak et al., 1985].

The vertical section along the 200-m isobath is shown in Figure 8. Slightly more vertical structure is seen near the shelf edge, particularly at midshelf regions near sites 8, 9, and 10, where the 1 cm s⁻¹ contour becomes horizontal. The maximum surface M2 tidal current amplitude is approximately 2.1 cm s⁻¹ at site 10 and 1.7 cm s⁻¹ at site 8. This is in qualitative agreement with *Rezak et al.* [1985] who saw evidence of a baroclinic M2 tidal current at the Flower Gardens Bank (close to

Table 4. O1 Tidal Current Ellipses at LATEX Current Meter Locations

Site Number	Depth, m	Hours	Major, cm s ⁻¹	Minor, cm s ⁻¹	θ, °N	G,
01	10.	10038.	0.33	-0.07	71.	2.
01	12.	5740.	0.45	-0.01	36.	35.
02	10.	15674.	1.39	-1.09	23.	179.
02 03	32.	9084.	0.95	-0.29	358.	121.
03	10. 33.	12808. 6268.	1.38	-1.25	34.	61.
03	53. 58.	7620.	1.32 0.73	-1.19 -0.53	34. 308.	7. 69.
04	14.	12345.	0.73	-0.33	22.	159.
04	100.	13258.	0.84	-0.67	333.	10.
04	190.	11807.	0.31	-0.10	289.	106.
05	14.	9310.	1.05	-0.68	68.	105.
05	100.	12405.	0.26	-0.20	344.	72.
05	190.	10596.	0.52	-0.19	315.	103.
06	14.	15136.	1.63	-1.44	7.	178.
06	100.	13447.	0.39	-0.16	85.	144.
06	190.	5949.	0.15	-0.02	71.	176.
07	14.	10982.	2.03	-1.60	46.	25.
07	100.	7224.	0.46	-0.22	357.	170.
07	190.	12800.	0.32	0.04	322.	16.
08	14.	15045.	1.44	-1.20	338.	103.
08	100.	12846.	0.51	-0.13	337.	65.
08	190.	11667.	0.37	-0.01	282.	122.
09 09	14. 100.	9933. 14413.	1.67	-1.00 -0.81	335.	105.
09 09	100. 190.	13013.	0.99 0.22	-0.81 -0.11	292. 29.	96. 161.
10	190.	10245.	1.48	-0.11 -1.01	29. 331.	161. 94.
10	100.	15473.	1.43	-0.83	333.	87.
10	190.	15406.	0.21	-0.83	76.	169.
11	14.	13752.	1.20	-0.68	335.	61.
11	100.	12746.	2.00	-1.31	313.	62.
11	190.	7113.	1.78	-0.43	322.	68.
12	14.	9798.	1.86	-0.89	76.	119.
12	100.	6230.	1.51	-1.04	299.	60.
12	490.	5401.	0.26	-0.09	82.	126.
13	14.	14328.	1.49	-0.63	89.	123.
13	100.	15725.	1.01	-0.46	275.	90.
13	190.	11357.	1.01	-0.49	76.	119.
14	10.	12287.	3.40	-2.46	72.	66.
14	26.	11257.	3.24	-2.51	274.	79.
14	40.	6895.	2.20	-1.30	88.	105.
15	10.	15708.	4.39	-3.39	87.	54.
15	17.	10509.	1.60	-0.60	281.	84.
16	10.	11879.	2.84	-1.90	90.	68.
16 17	14.	7653. 7406.	0.78	0.08	71.	54.
17	3. 6.	9382.	9.01 4.45	-4.04 -1.34	38. 35.	131. 140.
18	8.	11529.	3.91	-3.08	63.	152.
18	19.	9003.	0.77	-0.60	358.	77.
19	3.	7396.	2.41	-1.91	2.	82.
19	20.	6404.	2.27	-1.73	340.	68.
19	45.	9573.	1.47	-0.72	342.	86.
20	3.	10754.	2.87.	-1.55	355.	115.
20	13.	11457.	0.98	-0.03	327.	131.
21	14.	16245.	3.39	-2.83	5.	131.
21	22.	10681.	1.73	-1.09	349.	127.
22	3.	10356.	3.71	-3.23	15.	101.
22	20.	13677.	2.63	-2.22	0.	146.
22	48.	7849.	1.05	-0.74	9.	149.
23	10.	12342.	1.65	-0.77	70.	24.
23	13.	6043.	1.30	-0.51	65.	36.
24	10.	13028.	2.40	-1.41	44.	179.
24 25	25.	9939.	1.07	-0.75	81.	59.
25	11.	7705.	3.36	-2.73	60.	11.
25	20.	7851.	2.44	-1.98	61.	28.
	20	1050				
25 25	29.	4952.	2.34	-1.62 -1.07	53. 79	176. 102
	29. 13. 55.	4952. 3452. 2187.	2.34 1.84 0.77	-1.02 -1.07 -0.42	55. 79. 21.	1 /6. 102. 122.

Table 4. (continued)

Site Number	Depth, m	Hours	Major, cm s ⁻¹	Minor, cm s ⁻¹	θ, °N	G, ∘
46	50.	3271.	0.80	-0.65	22.	151.
46	84.	2164.	1.01	-0.57	27.	138.
48	14.	13556.	0.81	-0.13	357.	31.
48	100.	13519.	1.86	-1.15	330.	35.
48	190.	7204.	0.57	-0.02	317.	167.
49	14.	10618.	1.22	-1.03	317.	168.
49	100.	11523.	0.57	-0.42	10.	10.
49	490.	11341.	0.29	0.02	305.	18.

site 09). The M2 tidal current in the eastern and western portions of the 200-m isobath is nearly uniform throughout the water column.

3.2. Diurnal Tidal Currents

We define the diurnal energy band (22 - 28 hours) to contain the inertial periods found on the LATEX shelf as well as the principal diurnal tidal periods. As stated above, oscillating currents of diurnal periods dominate the current time series during the summer months on the Texas-Louisiana shelf. These currents are present during periods of high stratification and regular wind patterns (S. F. DiMarco et al., unpublished manuscript, 1997). These currents are seen to varying degrees at all mooring locations and depths and are the greatest at the midshelf surface records. To avoid contamination and interference of the diurnal oscillations with the K1 and P1 tidal estimates, all data recorded from June 1 through August 31 were removed from our analysis. Comparing the tidal amplitudes estimated with and without the summer data shows (1) all four of the semidiurnal estimates remain virtually unchanged, (2) the tidal energy contained in the two tides (O1 and Q1) which are appreciably far from a 24-hour period also are generally unchanged, and (3) the P1 and K1 tidal estimates (of 23.93 and 24.07 hours, respectively) are changed substantially. Specifically, the energy estimated in the P1 and K1 tides is reduced by an average of 37% and 27%, respectively, when the summer records are removed.

The O1 tidal component (period = 25.82 hours) ranges from 6% to 48% (average of 24.8%) of the total tidal variance and is the second largest tidal current component on the LATEX shelf. Table 4 lists the O1 tidal current parameters. The O1 tidal ellipses of the LATEX surface current meters are shown in Figure 9. The surface anticyclonically rotating O1 tidal current ellipses are more circular than the semidiurnal constituents. At the four sites (17, 19, 20, and 22) for which the upper current meter was at a depth of only 3 m, maximum amplitudes are larger than for other moorings with the upper instrument at 10 m. As we will see below, this is an indication of the strong vertical shear generally found in the diurnal tidal constituents.

The alignment of the tidal ellipses with respect to the bathymetry (when an orientation could be determined) is similar to that found in the semidiurnal constituents in that the semimajor axes of the ellipses were perpendicular to the bathymetry. Notable exceptions to this are again in the far east along 90.5°W, where the ellipses run parallel to the bathymetry, and sites 23 and 24, where the ellipses are essentially parallel to the coast. The latter two sites are located in a region where the shelf narrows.

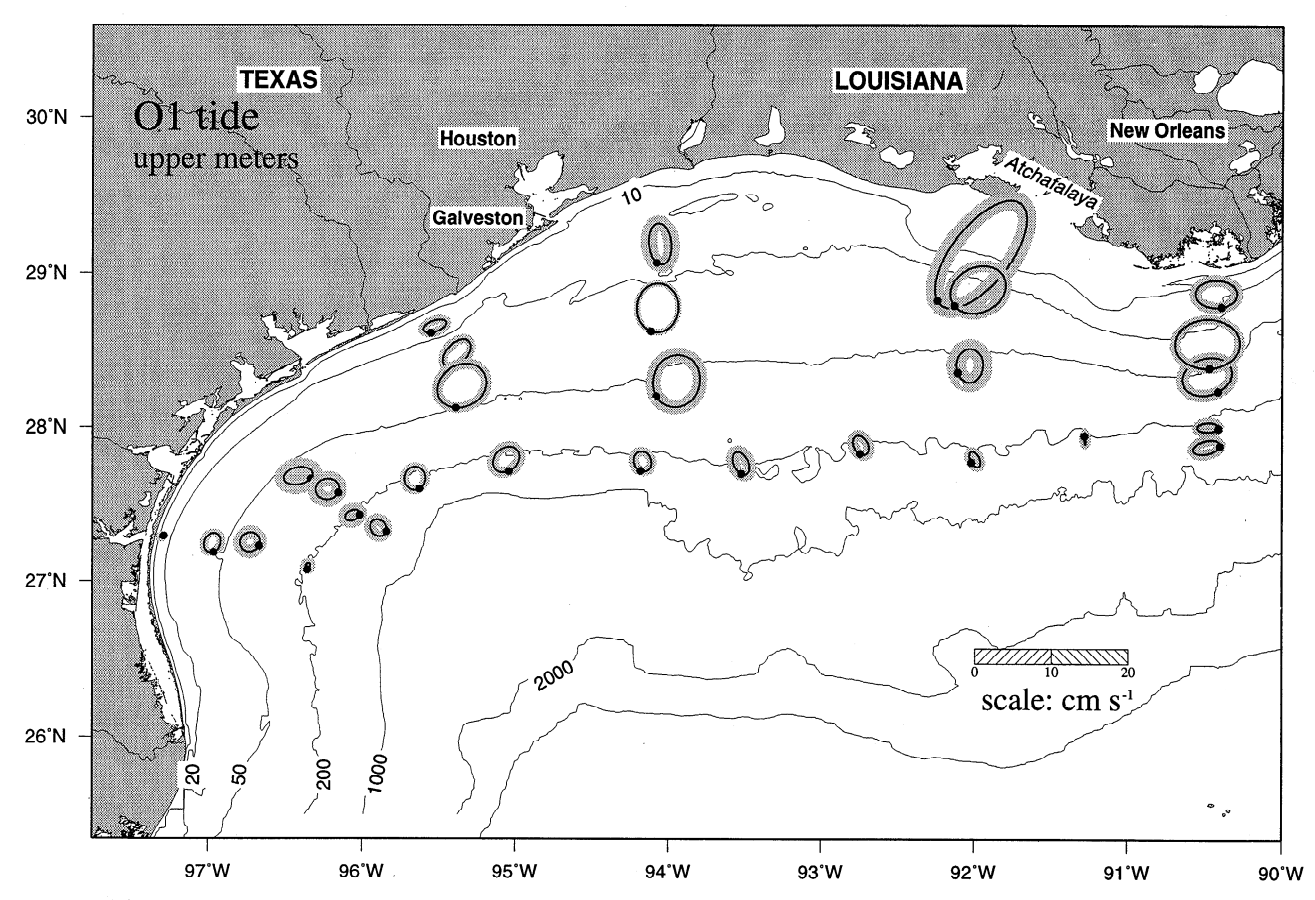


Figure 9. Mean O1 tidal current ellipses during the period April 1992 to December 1994 for upper current meters showing orientation of tidal current vectors at 0000 UTC, April 7, 1992 (solid circles) and least squares error estimate (shaded).

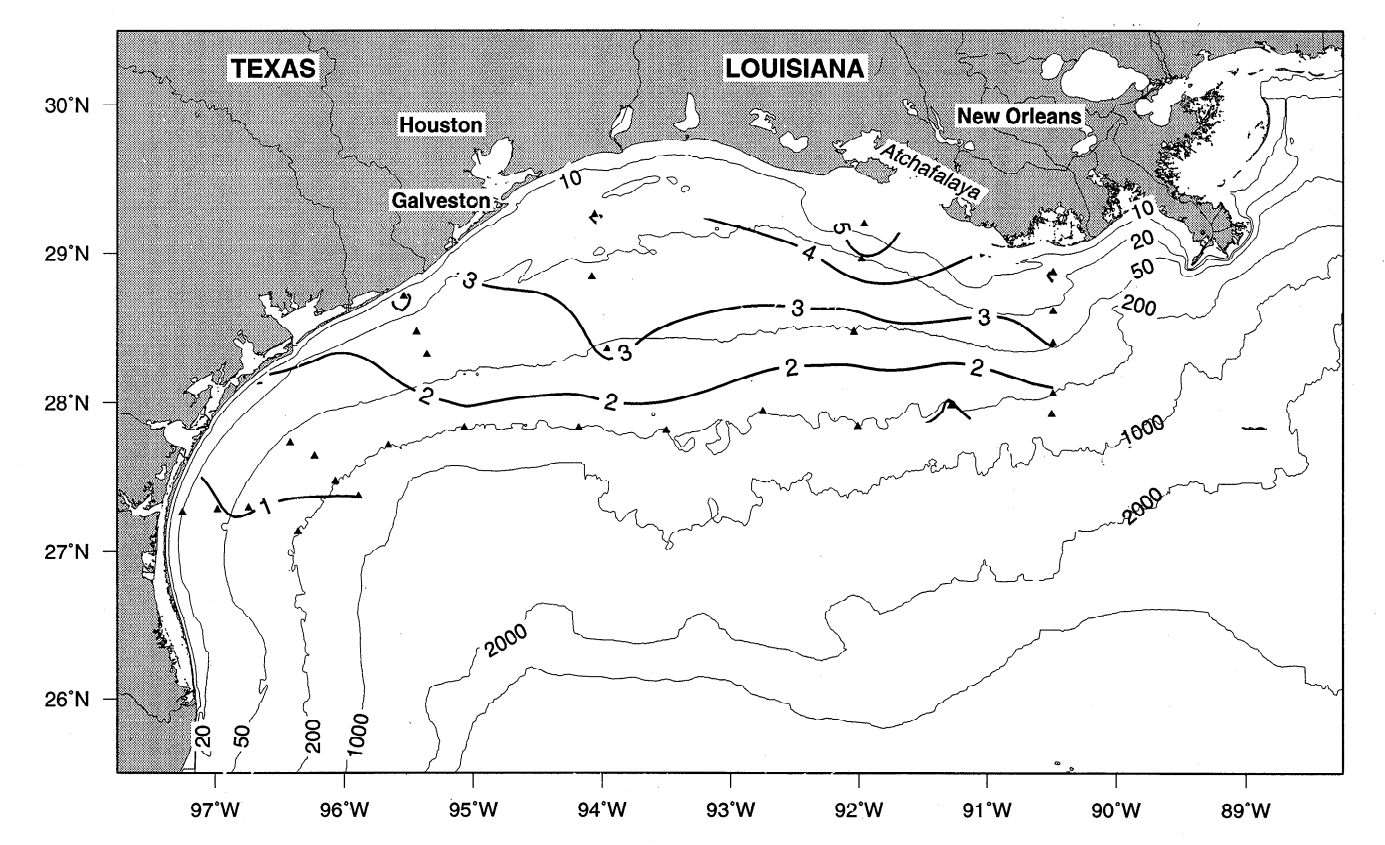


Figure 10. Contour of maximum O1 tidal current amplitudes for upper current meters. Triangles represent current meter locations. Contour interval is 1 cm s⁻¹.

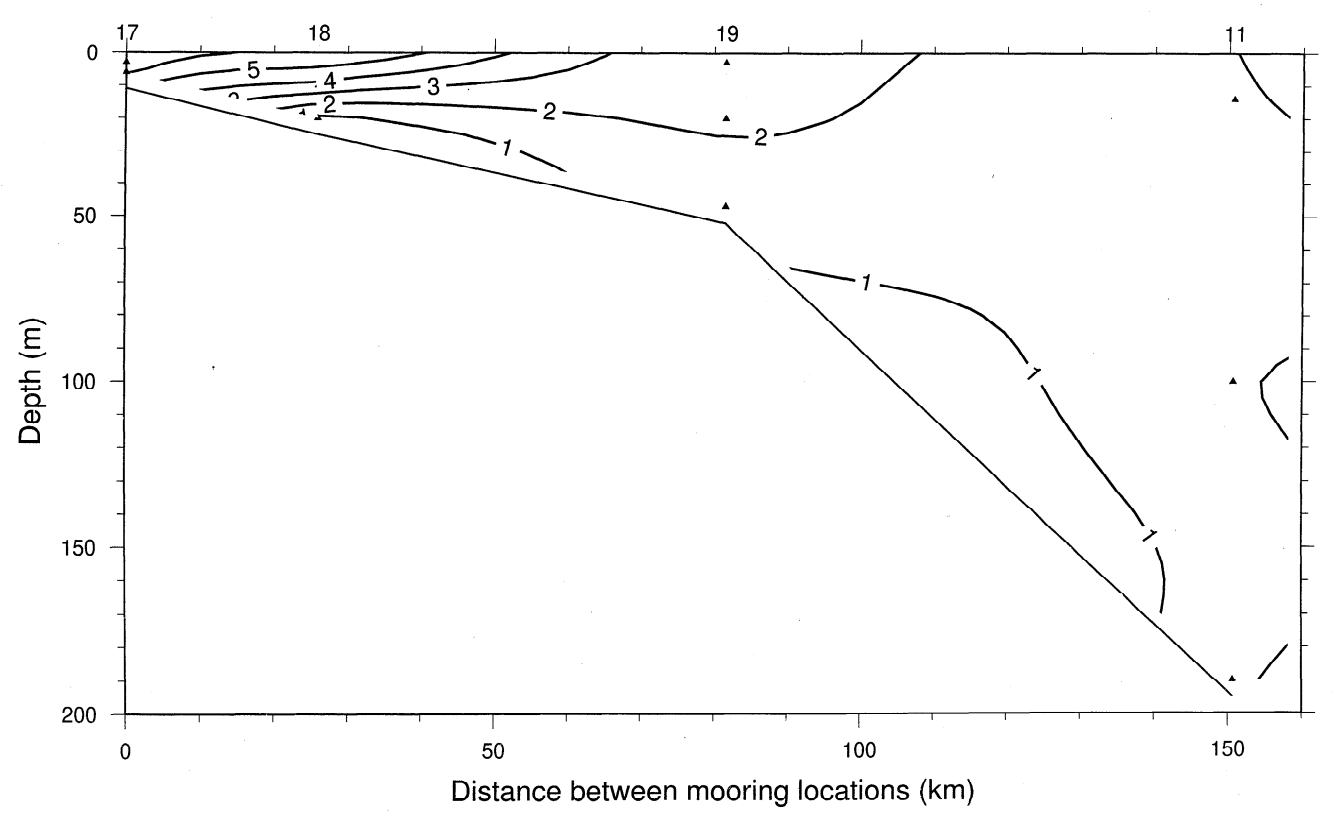


Figure 11. Vertical profile of maximum O1 tidal current amplitudes for current meters along 92°W. Triangles represent locations of current meters in water column. Mooring number is given at the top of the figure. Contour interval is 1 cm s⁻¹.

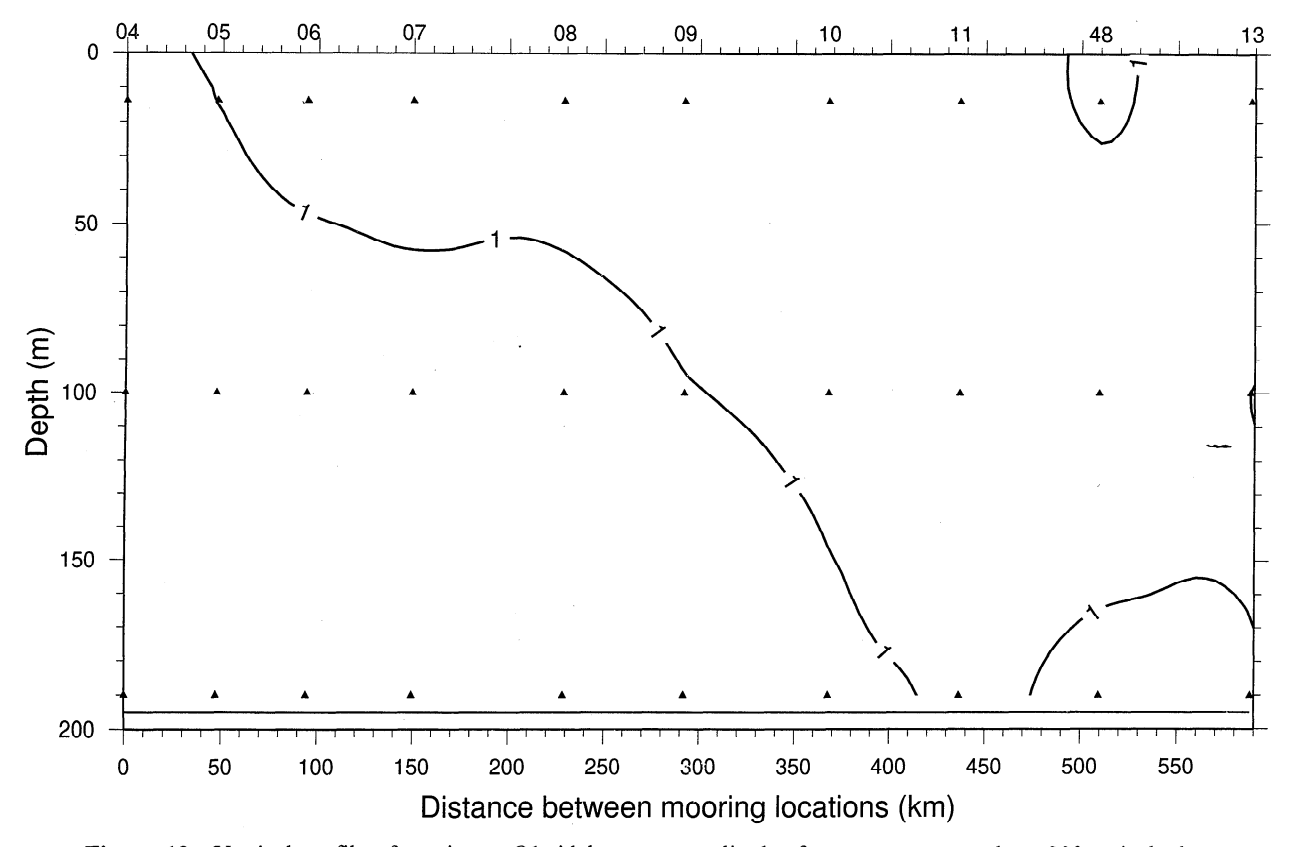


Figure 12. Vertical profile of maximum O1 tidal current amplitudes for current meters along 200-m isobath. Triangles represent locations of current meters in water column. Mooring number is given at the top of the figure. Contour interval is 1 cm s⁻¹.

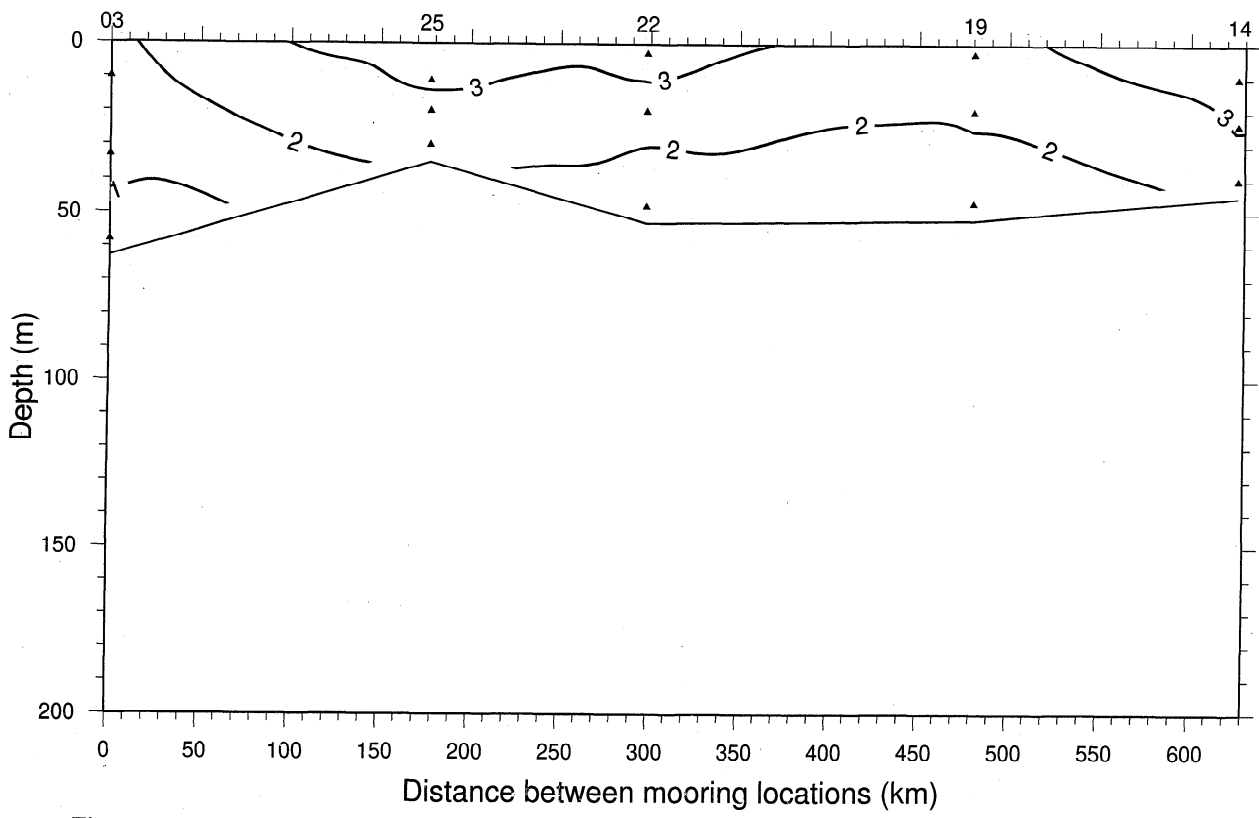


Figure 13. Vertical profile of maximum O1 tidal current amplitudes for current meters along 50-m isobath. Triangles represent locations of current meters in water column. Mooring number is given at the top of the figure. Contour interval is 1 cm s^{-1} .

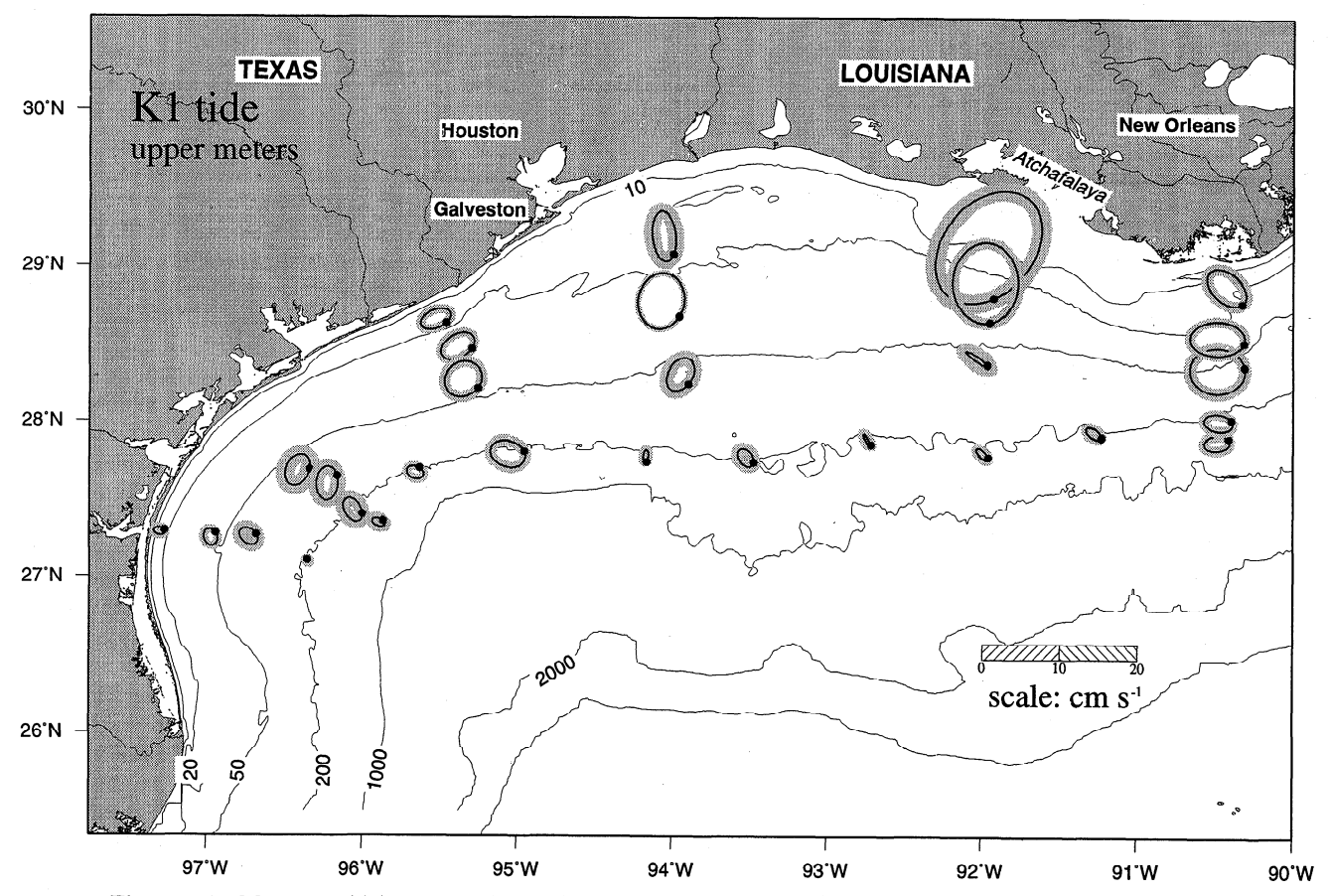


Figure 14. Mean K1 tidal current ellipses during the period April 1992 to December 1994 for upper current meters showing orientation of tidal current vectors at 0000 UTC, April 7, 1992 (solid circles) and least squares error estimate (shaded).

Table 5. K1 Tidal Current Ellipses at LATEX Current Meter Locations

G, Depth, Site Minor. θ. Hours Major, Number cm s⁻¹ cm s⁻¹ °N 01 10. 10038. 0.88 -0.63 288. 149. 01 12. 5740 0.87 -0.4317. 81. 02 10. 15674. 1.37 -1.08350. 17. 9084 -0.120. 02 32. 0.24 2. 03 10. 12808. 1.73 -1.61 338. 173. 03 33. 6268. 1.61 -1.33328. 154. 106. -0.56334. 03 58. 7620. 0.82 04 14. 12345. 0.84 -0.65336. 27. -0.56 288. 168. 04 100. 13258. 0.70 04 190. 11807 0.96 -0.68287. 52. 150. 05 9310. 1.52 -0.95320. 14. -0.70120. 05 100. 12405 0.92 303 0.59 -0.42331. 53. 05 190. 10596. 294. 157. 15136. 1.44 -1.1406 14. 149 06 100. 13447 0.25 -0.1526. 93. 06 190. 5949. 0.34 0.10 75. 10982. 291. 126. 07 2.33 -1.6114. 7224. 0.64 -0.47358. 119. 07 100. 12800. 0.43 -0.18121. 07 190. 38. 08 15045. 0.88 -0.14350. 122. 14. 107. 100. 12846. 2.26 -1.96322. 08 0.01 277. 120. 0.16 08 190. 11667. 09 9933. -0.67320. 118. 14. 1.32 119. 09 100. 14413. 1.45 -0.90332. 359. 115. -0.0909 190. 13013. 0.35 10245. 1.28 -0.42311. 127. 10 14. 15473. 2.99 -2.10340. 100. 100. 10 79 160. 190. 15406. 0.30 0.20 10 11 14. 13752. 1.49 -0.69314. 122. 100. 12746. 1.46 -0.76298. 111. 11 .37.11 190. 7113. 1.66 -0.756. 9798. 1.75 -1.0685. 114. 12 14. 6230. 0.47 0.39 289. 81. 100. 12 179. 12 490. 5401. 0.32 -0.073. 73. 100. 15725. 0.81 0.20 294. 13 146. 13 190. 11357. 0.78 -0.0724. -3.11 87. 90. 14 10. 12287. 3.87 14 26. 11257. 1.43 -0.5287. 87. 14 40. 6895. 1.42 -0.41 300. 56. 15 73. 10. 15708 3.71 -2.45270 15 10509. 40. 17. 0.74 0.14 287. 11879. -2.00 309. 76. 16 10. 3.29 16 14. 7653 1.01 -0.17336. 46. 17 7406. 130. 3. 8.77 -6.1637. 17 6. 9382. 5.28 -2.0434. 142. 18 8. 11529 5.24 -4.20359. 97. 19. 104. 18 9003 1.37 -0.3925. 19 308. 3. 7396. 2.83 -1.3595. 19 20. 6404. 2.39 -1.57 24. 110. 19 45. 9573. 2.17 -1.32346. 91. 20 10754. 3.49 117. 3. -1.56353. 20 13. 11457. 0.99 -0.04336. 121. 21 14. 16245. 3.86 -3.20150. 13. 21 22. 10681. -1.10137. 2.19 0. 22 3. 10356. 2.91 -1.9730. 154. 22 20. 13677. 2.45 -1.61 4. 131. 22 48 7849 1.83 -1.115. 116. 12342. 68. 31. 23 10. 2.23 -1.1023 -0.98341. 128. 13 6043 1.13 24 10. 13028. 2.86 -1.8754. 22. 24 25. 9939. 1.55 -1.1540. 4. 32. 25 2 57 -2 28 59 11. 7705 25 7851. 2.02 -1.46 36. 10. 20. 25 29. 4952. 2.07 -1.4533. 150. 34. 44 13. 3452 2.61 -1.8929 9. 44 55. 2187. 0.77 -0.65286. 2.59 5. 41. 4442 -1.7346 14 3271. -1.36 341. 104. 46 50. 1.86

Table 5. (continued)

Site Number	Depth, m	Hours	Major, cm s ⁻¹	Minor, cm s ⁻¹	θ, °N	G,
46	84.	2164.	0.76	0.17	72.	48.
48	14.	13556.	1.11	-0.45	307.	91.
48	100.	13519.	1.42	-0.61	340.	32.
48	190.	7204.	0.83	0.19	317.	10.
49	14.	10618.	1.28	-0.93	295.	162.
49	100.	11523.	0.87	-0.69	278.	115.
49	490.	11341.	0.67	-0.02	325.	63

The position of the O1 current vector at the time chosen in Figure 4 is again indicated by a solid circle on the tidal ellipses of Figure 9. The phase angle relative to the local bathymetry is more uniform across the shelf than the phase of the M2 tidal current, particularly along the 200-m isobath. The observed O1 ellipses and uniformity of the phase provide further verification of the *Reid and Whitaker* [1981] model on the shelf in that there is good relative agreement for the O1 current ellipse magnitude, orientation, and phase.

Figure 10 shows a contour plot of the maximum O1 tidal current amplitudes for the LATEX surface current meters (at depths of 10 m below the surface, except for sites 17, 19, 20, and 22 which are at a depth of 3 m below the surface). Here, the amplitudes are greatest near shore and decrease toward the shelf edge. The contours run essentially parallel to the isobaths at depths greater than 50 m. The O1 amplitudes also decrease where the western shelf bends to the south. As in the M2 tidal current, the maximum amplitude is located just south of Atchafalaya Bay.

Unlike the M2 tidal current ellipses, the O1 currents are not amplified in the wide shelf regions which also is in agreement with the CB model for tides on a continental shelf. The broad extent of the shallow shelf region south of the Atchafalaya Bay, however, contributes to the larger tidal amplitudes in that region for both the semidiurnal and diurnal constituents and also serves to rotate the axes of the tidal ellipse so that the semimajor axis is aligned perpendicular to the bathymetry. The Reid and Whitaker model has also shown both of these features in the region of the Atchafalaya [Rezak et al., 1985].

A vertical cross section of the maximum O1 tidal current amplitude along the 92°W meridian is shown in Figure 11. Apparent in this figure are the horizontal contours representing significant vertical shear past 100-m depth in the diurnal tidal currents. The shear is greatest near shore, as in the semi-diurnal cross sections, but extends across the 100-m isobath and close to the shelf edge. For sites 1-4, located at approximately 27.3°N, the currents are more homogeneous throughout the water column. However, Figure 11 is representative of the cross-shelf profile of all the diurnal tidal currents over the inner shelf east of 95.5°W.

In general, the diurnal tidal currents have greater shear than the semidiurnal tidal currents. However, the diurnal tidal ellipses are more circular, a result that would indicate that bottom friction may not be the primary cause of the shear since friction should cause the currents to become more rectilinear as the shear increases.

Figure 12 shows the maximum O1 tidal current amplitude at sites along the 200-m isobath. As in the M2 case (Figure 8), there is little vertical structure along the 200-m isobath. At

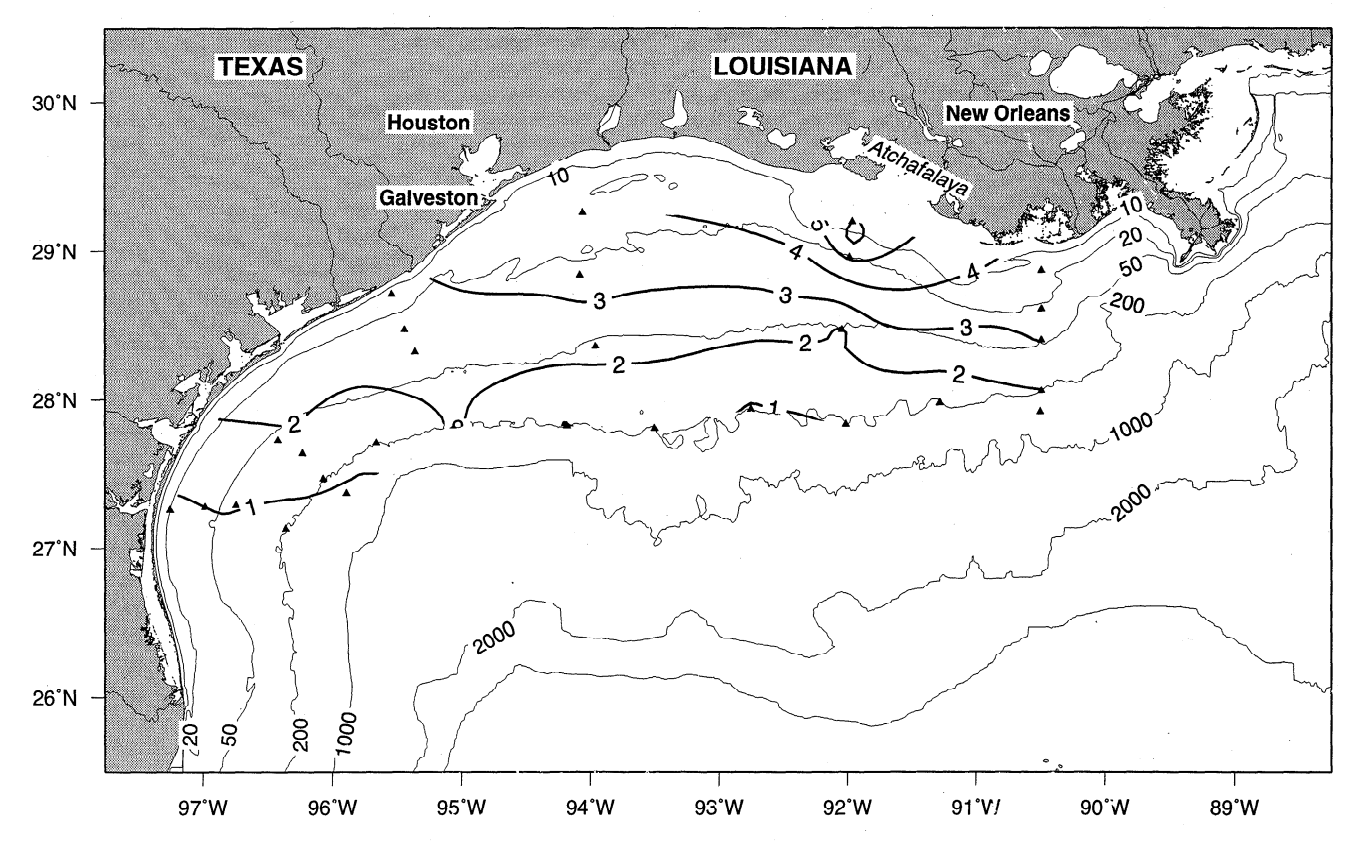


Figure 15. Contour of maximum K1 tidal current amplitudes for upper current meters. Triangles represent current meter locations. Contour interval is 1 cm s^{-1} .

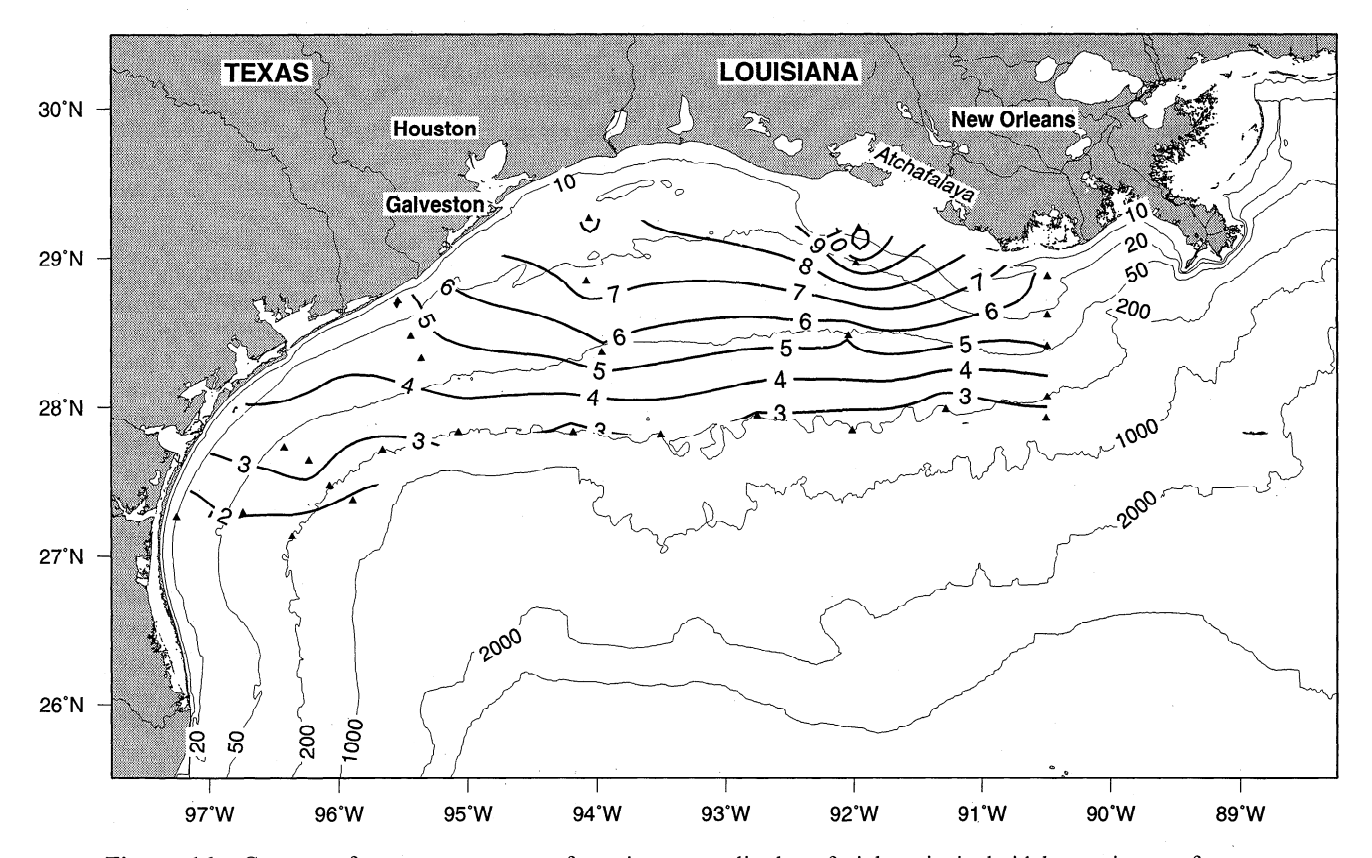


Figure 16. Contour of root-mean-square of maximum amplitudes of eight principal tidal constituents for upper current meters. Contour interval is 1 cm s⁻¹.

sites east of site 10, the O1 tidal current amplitudes are more barotropic and uniform with depth. This, however, does not continue to shallower depths, as analysis of the contours along the 50-m isobath (Figure 13) reveals strong vertical shear in the O1 tidal current on the eastern shelf.

The K1 tidal component ranges from 3% to 75% (average of 29%) of the total tidal variance and is therefore on average the largest tidal current component on the Texas-Louisiana shelf. Figure 14 shows the orientation of the surface K1 tidal current ellipses at each location. Table 5 lists the K1 tidal current parameters. Figure 15 shows a contour plot of the maximum K1 tidal current amplitude for the same meters shown in Figure 10. At the midshelf and eastern shelf regions, the maximum K1 amplitudes are similar to those found for the O1 tidal current. The K1 tide shows similar shear along the 50-m isobath and more shear along the 200-m isobath. As for the O1 tide, the phase of the K1 tide generally is uniform across the shelf.

The estimated tidal current amplitudes for the O1 (u amplitude of 2.02 cm s⁻¹ and v amplitude of 1.65 cm s⁻¹) and K1 (u amplitude of 2.84 cm s⁻¹ and v amplitude of 2.30 cm s⁻¹) tides for the surface meter at site 13 (instrument depth 14 m) compare reasonably well with the values reported by *Chen et al.* [1996] (O1 u velocity of 2.4 cm s⁻¹ and v velocity of 2.4 cm s⁻¹; K1 u velocity of 3.1 and v velocity of 2.6 cm s⁻¹). The latter estimates by *Chen et al.* [1996] were based upon 8-month records, which included summer data, and therefore overestimate the tidal currents for these two constituents. The estimates presented here are based on an effective record length of 20 months and include the nonsummer data analyzed by *Chen et al.* [1996].

The root-mean-square for all eight tidal current constituents of the upper current meters is shown in Figure 16. The figure can be regarded as representing amplitude associated with the average variance attributable to the eight principal tidal constituents. This figure shows that the tidal current amplitudes attributable to the principal tidal constituents are greatest at the wide central shelf regions between 91°W and 95°W. Amplitudes decrease along the narrow southward bending shelf region to the west. The largest amplitude is found near site 17 at Atchafalaya Bay. The amplitude isopleths run essentially parallel to the bathymetry between the 50- and 200-m isobaths. The variation of these amplitudes is primarily due to the combined effects of the wide shelf amplification processes of the semidiurnal constituents, stratification, and bottom friction.

3.3. Principal Tidal Sea Surface Height

Variations in sea surface height were estimated at five locations (sites 1, 16, 17, 20, and 23 in Figure 1) using bottom-mounted pressure gauges (Coastal Leasing, Inc., MiniSpec directional wave gauges). These gauges were positioned in water depths of 7 to 20 m. The sea surface height tidal constituents were estimated from the pressure time series using the method of cyclic descent. Table 6 summarizes the magnitude and phase (relative to Greenwich) for the five most energetic tidal constituents (M2, S2, K1, O1, and P1).

From Table 6, we see, for the M2 tidal phase, a lag between the western stations relative to stations in the east (consistent with the tidal current ellipse and the model study of *Reid and Whitaker* [1981]). This phase lag is also seen in the S2 tide. The phase for each of the diurnal constituents is essentially

Table 6. Magnitude and Phase of Principal Sea Surface Height Tidal Constituents at LATEX A Tide Gauge Locations

Site Number	Name	Period, hours	Magnitude, cm	G,

16	M2	12.42	2.5	172
17	M2	12.42	10.3	239
20	M2	12.42	16.8	265
23	M2	12.42	8.5	268
01	M2	12.42	7.9	260
16	S2	12.00	1.9	129
17	S2	12.00	3.1	218
20	S2	12.00	4.8	252
23	S2	12.00	1.7	245
01	S2	12.00	1.6	233
16	K1	23.93	16.2	15
17	K1	23.93	16.1	21
20	K1	23.93	16.9	28
23	K1	23.93	15.4	25
01	K1	23.93	16.3	25
16	O 1	25.82	14.7	10
17	O1	25.82	15.5	14
20	01	25.82	15.9	17
23	O1	25.82	14.8	16
01	O1	25.82	14.9	16
16	P1	24.07	4.4	35
17	P1	24.07	4.7	31
20	P1	24.07	4.4	27
23	P1	24.07	3.5	37
01	P1	24.07	4.0	46

uniform across the shelf. Also evident is the amplification of the semidiurnal magnitudes at the midshelf locations, particularly at mooring 20.

To obtain a rough estimate for the amount of amplification of the semidiurnal tidal height amplitudes that is predicted by CB theory for the Texas-Louisiana shelf, we applied some realistic values for the physical characteristics of the shelf at 90.5°W and 94°W in the CB equations for $\eta(0)/\eta(L)$, where $\eta(0)$ and $\eta(L)$ are the surface height for a given constituent at the coast and at the shelf edge, respectively. This estimate is rough because CB theory does not take into account some important factors that can influence tidal dynamics, such as irregular coastlines and frictional and topographic effects, characteristics that the Texas-Louisiana shelf possesses. For the semidiumal constituents, the ratio of $\eta(0)/\eta(L)$ for 90.5°W and 94°W is 0.28. For the diurnal constituents, the ratio is 1.0. From Table 6, the M2 and S2 tidal height amplitude ratio at site 16 to site 20 is 0.15 and 0.40, respectively. For the diurnal constituents the ratios are 0.96, 0.92, and 1.00, for the K1, O1, and P1 tides, respectively. Therefore, CB theory is generally consistent with the observations of tidal height on the Texas-Louisiana shelf.

The tidal amplitudes listed above compare well with historical values recorded at five locations [Capurro and Reid, 1972] that lie in close proximity to LATEX A mooring locations. For example, the tidal amplitudes for a station at 29.78°N, 93.35°W (near site 20) are 16, 5, 14, and 13 cm, for the M2, S2, K1, and O1 tides, respectively.

4. Summary and Conclusions

We have analyzed the eight principal tidal current constituents at 31 sites on the LATEX shelf during nonsummer months. Along the shelf break during this period, the energy attributable to the tidal currents accounts for roughly 10% of the total variance in the 8- to 40-hour energy band of the spectrum. The percentage of tidal energy increases to 50% near shore.

The semidiurnal tidal current constituents for surface meters have ellipses with current vectors that generally rotate anticyclonically and, with few exceptions, have major axes that lie across bathymetric lines. Vertical cross sections show that these tidal currents are essentially barotropic except for the near-shore locations (20-m depth and less) where bottom friction and stratification are believed to produce shear. The currents are generally larger at the middle shelf due to the amplification process of the wide shelf.

The diurnal tidal current constituents for surface meters have ellipses that are circular and also rotate anticyclonically. Vertical shear is present in the cross sections throughout the shelf region and extends to the 200-m isobath. The tidal amplitudes are generally uniform for locations at constant depth and only increase slightly in magnitude near shore.

A synoptic view of the orientation of the tidal current vectors of each constituent suggests that the M2 tidal current propagates cyclonically (east to west) along the shelf, while the O1 and K1 tides are nearly in phase along the shelf.

The amplitude, phase, and orientation of the tidal current ellipses also provide some qualitative verification of the Gulf of Mexico model by *Reid and Whitaker* [1981] in the region of the Texas-Louisiana shelf.

Acknowledgments. This study was funded by the U.S. Minerals Management Service under OCS contract 14-35-0001-30509. Additional funding has been provided by Texas A&M University, the Texas Engineering Experiment Station, and the Texas Institute of Oceanography. We would like to thank the two anonymous reviewers of the original manuscript for their thoughtful and insightful recommendations and comments. Maps and contouring were produced using the Generic Mapping Tools (GMT) software package [Wessel and Smith, 1995].

References

Bloomfield, P., Fourier Analysis of Time Series: An Introduction, pp. 22-41, John Wiley, New York, 1976.

Capurro, L, R. A., and J. L. Reid (Eds.), Contributions on the Physical Oceanography of the Gulf of Mexico, vol. 2, 288 pp. Tex. A&M Univ., Oceanogr. Stud., Gulf, Houston, Tex., 1972.

- Chen, C., R. O. Reid, and W. D. Nowlin, Jr., Near-inertial oscillations over the Texas-Louisiana shelf, *J. Geophys. Res.*, 101(C2), 3509-3524 1996
- Clarke, A. J., and D. S. Battisti, The effect of continental shelves on tides, *Deep Sea Res.*, 28A, 665-682, 1981.
- Foreman, M. G. G., Manual for tidal heights analysis and prediction, *Pac. Mar. Sci. Rep.* 77-10, 97 pp., Inst. of Ocean Sci., Patricia Bay, Sidney, B.C., Canada, 1977.
- Foreman, M. G. G., W. R. Crawford, and R. F. Marsden, Detiding: Theory and practice, in *Quantitative Skill Assessment for Coastal Ocean Models, Coastal Estuarine Stud.*, vol. 47, edited by D. R. Lynch and A. M. Davies, pp. 203-239, AGU, Washington, D.C., 1995.
- Godin, G., The Analysis of Tides, 264 pp., Univ. of Toronto Press, Toronto, Ont., Canada, 1972.
- Gonella, J., A rotary-component method for analysing meteorological and oceanographic vector time series, *Deep Sea Res.*, 19, 833-846, 1972
- Li, Y., W. D. Nowlin, Jr., and R. O. Reid, Mean hydrographic fields and their interannual variability over the Texas-Louisiana continental shelf in spring, summer, and fall, J. Geophys. Res., 102(C1), 1027-1049, 1997.
- Marmer, H. A., Tides and sea level of the Gulf of Mexico, in *Gulf of Mexico: Its origin, waters, and marine life, Fish. Bull. 89, Fish. Bull. Fish Wild. Serv.* 55, 101-118, 1954.
- Mofjeld, H. G., and M. Wimbush, Bottom pressure observations in the Gulf of Mexico and Caribbean Sea, *Deep Sea Res.*, 24, 987-1004, 1977.
- Price, J. F., R. A. Weller, and R. Pinkel, Diurnal cycling: Observations and models of the upper ocean response to diurnal heating, cooling, and wind mixing, J. Geophys. Res., 91(C7), 8411-8427, 1986.
- Reid, R. O., Tides and storm surges, in *Handbook of Coastal and Ocean Engineering*, vol. I, edited by J. B. Herbick, pp. 533-590, Gulf, Houston, Tex., 1990.
- Reid, R. O., and R. E. Whitaker, Numerical Model for Astronomical Tides in the Gulf of Mexico, vol. I, Theory and Application, 115 pp. Tex. A&M Univ., College Station, Tex., 1981.
- Rezak, R., T. J. Bright, and D. W. McGrail, Reefs and Banks of the Northwestern Gulf of Mexico, 259 pp., John Wiley, New York, 1985.
- Schureman, P., Manual of Harmonic Analysis and Predictions of Tides, Coast Geod. Surv. Spec. Publ. 98, U.S. Dep. of Commerce, Washington, D.C., 1976.
- Wessel, P., and W. H. F. Smith, New version of the Generic Mapping Tools released, *EOS Trans. AGU, 76*, 329, 1995.

(Received February 4, 1997; revised August 8, 1997; accepted September 15, 1997.)

S. F. DiMarco and R. O. Reid, Department of Oceanography, Texas A&M University, College Station, TX 77843-3146. (c-mail: dimarco@latexa.tamu.edu)